

The Three-Dimensional Shapes of Galaxy Clusters

Marceau Limousin, Andrea Morandi, Mauro Sereno, Massimo Meneghetti, Stefano Ettori, Matthias Bartelmann & Tomas Verdugo

Received: date / Accepted: date

Abstract While clusters of galaxies are considered one of the most important cosmological probes, the standard spherical modelling of the dark matter and the intracluster medium is only a rough approximation. Indeed, it is well established both theoretically and observationally that galaxy clusters are much better approximated as triaxial ob-

Marceau Limousin
Aix Marseille Université, CNRS, LAM (Laboratoire d'Astrophysique de Marseille) UMR 7326,
13388, Marseille, France
E-mail: marceau.limousin@oamp.fr
&
Dark Cosmology Centre, Niels Bohr Institute, University of Copenhagen
Juliane Maries Vej 30, DK-2100 Copenhagen, Denmark
E-mail: marceau.limousin@oamp.fr

Andrea Morandi
Raymond and Beverly Sackler School of Physics and Astronomy, Tel Aviv University, Tel Aviv,
69978, Israel

Mauro Sereno
Dipartimento di Fisica, Politecnico di Torino, corso Duca degli Abruzzi 24, 10129 Torino, Italy
&
INFN, Sezione di Torino, via Pietro Giuria 1, 10125, Torino, Italy

Massimo Meneghetti
INAF - Osservatorio Astronomico di Bologna, via Ranzani 1, 40127, Bologna, Italy &
INFN, Sezione di Bologna, Viale Bertini Pichat 6/2, 40127, Bologna, Italy

Stefano Ettori
INAF - Osservatorio Astronomico di Bologna, via Ranzani 1, 40127, Bologna, Italy &
INFN, Sezione di Bologna, Viale Bertini Pichat 6/2, 40127, Bologna, Italy

Matthias Bartelmann
Zentrum für Astronomie, Institut für Theoretische Astrophysik, Albert-Überle Str. 2, 69120,
Heidelberg, Germany

Tomas Verdugo
Centro de Investigaciones de Astronomía (CIDA), Apartado Postal 264, Mérida 5101-A,
Venezuela

jects. However, investigating the asphericity of galaxy clusters is still in its infancy. We review here this topic which is currently gathering a growing interest from the cluster community. We begin by introducing the triaxial geometry. Then we discuss the topic of deprojection and demonstrate the need for combining different probes of the cluster's potential. We discuss the different works that have been addressing these issues. We present a general parametric framework intended to simultaneously fit complementary data sets (X-ray, Sunyaev Zel'dovich and lensing data). We discuss in details the case of Abell 1689 to show how different models/data sets lead to different haloe parameters. We present the results obtained from fitting a 3D NFW model to X-ray, SZ, and lensing data for 4 strong lensing clusters. We argue that a triaxial model generally allows to lower the inferred value of the concentration parameter compared to a spherical analysis. This may alleviate tensions regarding, *e.g.* the over-concentration problem. However, we stress that predictions from numerical simulations rely on a *spherical analysis* of triaxial halos. Given that triaxial analysis will have a growing importance in the observational side, we advocate the need for simulations to be analysed in the very same way, allowing reliable and meaningful comparisons. Besides, methods intended to derive the three dimensional shape of galaxy clusters should be extensively tested on simulated multi-wavelength observations.

Keywords Cosmology · Galaxy Clusters · Triaxiality · Gravitational Lensing · X-rays · Sunyaev Zel'dovich

1 Three-Dimensional Shape of Galaxy Clusters

Spectroscopic galaxy redshift surveys and numerical N-body simulations have revealed a large scale distribution of matter in the Universe featuring a complex network of interconnected filamentary galaxy associations. Vertices, i.e. intersections among the filaments, correspond to the very dense compact nodes within this *cosmic web* where one can find massive galaxy clusters.

In this review, we concentrate on the shape of galaxy clusters.

1.1 Galaxy Clusters are *not* Spherical

There is much observational evidence for clusters not being spherical objects, from the non-circular projection of various probes: optical, from the density maps of cluster galaxies (Carter and Metcalfe 1980; Binggeli 1982); X-ray, from the surface brightness maps (Fabricant et al. 1984; Buote and Canizares 1992, 1996; Kawahara 2010; Lau et al. 2012); Sunyaev Zel'dovich pressure maps (Sayers et al. 2011a); strong gravitational lensing (Soucail et al. 1987), and weak gravitational lensing (Evans and Bridle 2009; Oguri et al. 2010, 2012). Recently, the azimuthal variation of galaxy kinematics has been detected for the first time in a stacked sample of 1 743 galaxy clusters from the SDSS (Skielboe et al. 2012). They find that the line of sight velocity dispersion of galaxies lying along the major axis of the central galaxy is larger than those that lie along the minor axis. This detection provides further evidence for the asphericity of galaxy clusters.

On the numerical side, haloes forming in cosmological simulations have been found to be triaxial in shape, with a preference for prolateness over oblateness (Frenk et al. 1988; Dubinski and Carlberg 1991; Warren et al. 1992; Cole and Lacey 1996; Jing and Suto

2002; Hopkins et al. 2005; Bailin and Steinmetz 2005; Kasun and Evrard 2005; Paz et al. 2006a; Allgood et al. 2006; Bett et al. 2007; Muñoz-Cuartas et al. 2011; Gao et al. 2012). These simulations also predict an evolution of the shape with mass and redshift: low mass haloes appear more spherical than high mass haloes (see, however, an opposite conclusion by Rossi et al. 2011), and for a given mass, lower redshift haloes are more spherical than high redshift haloes.

However, more than forty years after the first observational evidence of the asphericity of galaxy clusters, the majority of cluster studies use the spherical assumption. Historically, this was due to the fact that the quality of the data may not allow a triaxial model to be constrained. Besides, studies often rely on the analyses of a single data set (*e.g.* lensing, X-ray, SZ or dynamics of cluster members only), while to recover triaxiality one needs to combine data sets, unless some priors are used (see Section 2).

Besides the expectation for triaxial collapse coming from first principles (see Section 1.2), another hint regarding the need for non-spherical models is the mass discrepancy found between, *e.g.* lensing and X-ray data when spherical symmetry is assumed (Piffaretti et al. 2003; Clowe et al. 2004; Gavazzi 2005; Corless and King 2007).

1.2 Triaxiality: a Consequence of Gravitational Collapse for an Initial Gaussian Random Field of Density Fluctuations

Interestingly, triaxial collapse is a straightforward prediction of structure growth driven by self-gravity of Gaussian density fluctuations. Well into the mildly non-linear regime, gravitational structure formation can be described by the Zel'dovich approximation, which models the motion of dark-matter particles as inertial motion in a suitably adapted time coordinate. This assumption defines a map between initial, Lagrangian, and final, Eulerian coordinates of any particle. The Jacobian of this map is called the Zel'dovich deformation tensor, here abbreviated as F . The matter density is then simply given by the inverse determinant of F , times the initial density.

Under the (reasonable) assumption of an initially irrotational flow, a velocity potential ψ exists in Lagrangian space whose gradient is the Lagrangian velocity field. The Zel'dovich deformation tensor can be represented by the unit matrix plus the Hessian (curvature) matrix of the velocity potential,

$$F_{ij} = \delta_{ij} + \partial_i \partial_j \psi. \quad (1)$$

It is thus symmetric and has three real eigenvalues $(1 + \lambda_i)$, $i = 1, 2, 3$.

Since determinants are invariant under orthogonal transforms, the inverse determinant of the Zel'dovich tensor is

$$(\det F)^{-1} = \left[\prod_{i=1}^3 (1 + \lambda_i) \right]^{-1}. \quad (2)$$

Collapse will set in according to the Zel'dovich approximation whenever any of the eigenvalues λ_i approaches -1 . If all eigenvalues λ_i were the same, collapse was spherical; if they were all different, collapse was triaxial.

It was shown already by Doroshkevich (1970) that the probability distribution for the λ_i in a Gaussian random field is proportional to the product of absolute differences

$$|\lambda_i - \lambda_j| \quad (3)$$

for any pair i, j with $j \neq i$. This means that equal eigenvalues are not allowed in a Gaussian random field, thus excluding spherical and even spheroidal collapse: in any realistic triple of eigenvalues, no pair of them can be equal. Collapse will proceed first along the principal axis belonging to the largest eigenvalue, forming the sheet-like structures called ‘pancakes’ by Zel’dovich. Those will then contract along the principal axis of the second-largest eigenvalue, forming essentially one-dimensional bridges of matter that finally shrink to triaxial haloes along their remaining axis. This inherent and necessary triaxiality of the mildly non-linear collapse is retained through the non-linear collapse of the haloes which is stopped by virialization.

1.3 Triaxiality: an Outgrowth of the Large Scale Structure Formation Scenario

The standard cosmological framework (Λ CDM), which consists of a cosmological constant and cold dark matter (DM) with Gaussian initial conditions, envisages structure formation as a hierarchical merging process. With this perspective, gravity is constantly pulling lumps of matter together to form increasingly larger structures. The structures we see in the Universe today (galaxies, clusters, filaments, sheets and voids) are predicted to have formed in this way, with galaxy clusters sitting atop this hierarchy and being the largest virialized structures that have had time to collapse under the influence of their own gravity. In particular, being a tracer of the primordial density perturbations, this large scale structure scenario leads to a picture where the matter is distributed as a network of gigantic dense (filaments) and empty (voids) regions, creating a vast foam-like structure called the “cosmic web”, with the densest regions of the dark matter cosmic web hosting massive clusters of galaxies. Numerical simulations, in agreement with analytic predictions, indicate that the infall of material into the most massive dark matter haloes is not spherical but is expected to be preferentially funnelled through the filaments where the haloes are embedded. The cluster mass haloes would indeed acquire most of their mass from major mergers along the filaments, hence leading to an alignment between the major axis of the host halo and the large-scale filament (Bailin and Steinmetz 2005; Altay et al. 2006; Patiri et al. 2006; Aragón-Calvo et al. 2007; Brunino et al. 2007). Clusters would then relax from this chaotic initial state to a quasi-equilibrium via violent relaxation. This process leads to equilibrium which is plausibly related to bounded triaxial DM distribution with a ‘universal’ density structure, regardless of halo mass, of cosmological parameters, and of the initial fluctuation spectrum. Therefore, triaxiality appears to be a direct outgrowth of the large scale structure formation scenario, providing a record of the initial conditions in the Universe and of the topology of the cosmic structures.

2 From 2D Observables to a 3D Mass Model: Deprojection

2.1 An Under-Constrained Problem

The problem of deprojection is typically under-constrained: we have access to 2D projected informations (X-ray surface brightness maps, or lensing mass density maps) and aim to derive the 3D properties of the triaxial structure.

As an example, let’s consider gravitational lensing observations. Fitting triaxial models with lensing data only is an intrinsically under-constrained problem, since lens-

ing can never give full information about the 3D triaxial structure: it is constraining only the 2D projected mass density. This translates into much larger error bars on the parameters of a triaxial halo constrained using lensing observations alone. These error bars fairly represent the true extent of our limited knowledge of the structure of galaxy cluster lenses, and make clear the importance of combining constraints from other theoretical or other observational data in order to narrow down the parameter space of a more realistic triaxial model.

The first attempts to determine three dimensional morphologies were based on statistical approaches consisting in the inversion of the distribution of apparent shapes. Hubble (1926) first determined the relative frequencies with which galaxies of a given intrinsic ellipticity, oriented at random, are observed as having various apparent projected ellipticities. Several following studies have then applied similar methods to different classes of astronomical objects (Noerdlinger 1979; Binggeli 1980; Binney and de Vaucouleurs 1981; Fasano and Vio 1991; de Theije et al. 1995; Mohr et al. 1995; Basilakos et al. 2000; Cooray 2000; Thakur and Chakraborty 2001; Alam and Ryden 2002; Ryden 1996; Plionis et al. 2004; Paz et al. 2006b). With the exception of disc galaxies, prolate-like shapes appear to dominate all cosmic structure on a large scale.

2.2 Combining Data Sets

We will consider three different types of data sets: gravitational lensing (both weak and strong), X-ray emission, and the thermal SZ effect. For details on these different data sets, we refer the reader to the other reviews published in this volume.

When combining X-ray and SZ data sets, the idea is that one can infer the 3D properties of a cluster by taking advantage of the different dependences of the X-ray and SZ signals on the gas density and temperature: the SZ effect is proportional to the electron pressure integrated along the line of sight, whereas the X-ray surface brightness is proportional to the integral along the line of sight of the square of the electron density. Besides, gravitational lensing provides a direct probe of the two dimensional mass distribution projected along the line of sight.

Combining complementary data sets to reconstruct the three dimensional properties of galaxy clusters is not a new idea, and different authors have proposed different approaches.

2.2.1 Theoretical Studies

We review here the works that have developed methods which have been tested on simulated data sets only.

Zaroubi et al. (1998) proposed a non parametric deprojection method specifically designed for the deprojection of X-ray, SZ and lensing maps of galaxy clusters, under the assumption of *axial symmetry* of the cluster. This method was first applied to a simple analytic model for cluster dark matter and gas distributions, then it was tested on cosmological hydrodynamical simulations of galaxy clusters (Zaroubi et al. 2001). The authors found a good agreement between the actual (simulated) and reconstructed three-dimensional properties.

Some studies proposed a non parametric deprojection method based on Abel's integrals. This inversion is applied on SZ and X-ray data in order to infer temperature and density profiles of the ICM. Silk and White (1978) were the first to propose to apply

the Abel inversion to the X-ray and SZ profiles, but their approach was limited to the estimation of the central values of gas density and temperature aiming at the determination of cosmological parameters. More recently, Yoshikawa and Suto (1999) used this technique for a non parametric reconstruction of radial density and temperature profiles using analytical and simulated cluster models. This method assumes *spherical symmetry*, and Yoshikawa and Suto (1999) mention the inclusion of non-spherical effects as an important next step.

Reblinsky (2000) developed a non parametric algorithm for the simultaneous deprojection of X-ray, weak lensing, and SZ data. They specify a geometrical model for the cluster assuming *axial symmetry*. Using gas-dynamical simulations, they demonstrated the quality of the deprojections.

Later, Puchwein and Bartelmann (2006) proposed a method based on Richardson-Lucy deconvolution to reconstruct the three-dimensional gas density and temperature distributions in galaxy clusters from combined X-ray and SZ observations. They tested their algorithm against synthetic observations using both analytically and fully numerically simulated clusters. They found that their method reconstructs the gas density and temperature distributions accurately in three-dimensions, even if observational noise is present. Additionally, they discussed a method to constrain the cluster inclination along the line of sight using X-ray temperature maps. They came to the conclusion that the method allows to reach a level of accuracy of $\sim 15\%$.

Fox and Pen (2002) considered the problem of deprojecting aspherical clusters. They first constructed a parametrised 3D *axisymmetric* cluster model, and determined the 3D cluster shapes using a χ^2 fitting between the model predictions and the simulated data.

Marshall et al. (2003) presented a Bayesian joint analysis of cluster weak lensing and SZ data, assuming *spherical symmetry*. This methodology was applied to two sets of simulated SZ and weak lensing data sets.

Lee and Suto (2004) considered a deprojection method combining SZ and X-ray data and applied it to analytical cluster models, considering *triaxial haloes* with constant axis ratios.

Ameglio et al. (2007, 2009) presented deprojection methods (parametric as well as non parametric) in order to recover the three dimensional density and temperature profiles by combining SZ and X-ray surface brightness maps, assuming the cluster to be *spherically symmetric*. They apply their techniques to a set of hydrodynamical simulations of galaxy clusters in order to estimate the biases and scatters on the recovered masses.

Allison et al. (2011) proposed a parametrised *spherical* model of the intracluster medium aimed for jointly analysing SZ and X-ray data. This entropy based model which relies on the assumption of hydrostatic equilibrium is tested against mock observations of clusters from N-body/hydrodynamic simulations.

Samsing et al. (2012) presented a novel method for measuring a radially dependent shape along the line of sight of the ICM from the X-ray observations only. The method hinges on the assumption that the shapes, temperature and density profiles can be described by parametrised functions. This model generates fake spectra to be compared with the observed spectral information. A clear advantage of this approach is that it does not require any combination with independent measurements of *e.g.* the cluster mass or density profile. The major downside for the current observations is that it requires data of impressively high quality ($\sim 10^6$ photons) to get a 5σ detection of the shape.

2.2.2 Observational Studies

As seen before, from their different dependencies on the density, combining X-ray and SZ allows us to directly infer the elongation of the gas distribution. No assumption is needed about hydrostatic equilibrium. The method exploits X-ray spectroscopic and photometric data plus measurements of the Sunyaev-Zel'dovich effect. One needs to deproject the X-ray and SZ data. Both data sets are supposed to trace the same temperature (remember that SZ gives a mass weighted temperature, unlike X-ray), and one assumes that no clumpiness and no contamination from structures along the line of sight might bias the SZ data. The gas distribution is modelled with an ellipsoidal parametric profile which can fit the observed X-ray surface-brightness and temperature. Comparison with the SZ amplitude fixes the elongation along the line of sight e_{Δ} . For an isothermal plasma (De Filippis et al. 2005),

$$e_{\Delta} \propto D_d \frac{SB}{\Delta T_{SZ}^2} \frac{T^2}{\Lambda_X} \quad (4)$$

where D_d is the angular diameter distance to the cluster, SB is the surface brightness, ΔT_{SZ} the SZ temperature decrement, T the temperature, and Λ_X the emissivity. Finally, Bayesian inference allows us to deproject the measured elongation and the projected ellipticity measured in the plane of the sky, in order to constrain the intrinsic shape and orientation of the cluster.

This approach was first employed in De Filippis et al. (2005), who considered a sample of 25 X-ray luminous clusters. They used parametric *ellipsoidal profiles* of constant eccentricities aligned along the line of sight, assuming an isothermal beta model parametrisation for the ICM. They found that the spherical hypothesis is strongly rejected for most of the 25 clusters of the X-ray selected sample studied. Considering the same data but assuming *axial symmetry*, Sereno et al. (2006) showed that this sample is composed of a mixed population of prolate and oblate haloes, with prolate shapes preferred in ~ 60 -76% of the cases. They observe an excess of clusters elongated along the line of sight, with respect to what is expected from a randomly oriented cluster population. They claim that a more general triaxial morphology might better describe the morphology of these clusters. Both studies acknowledged that adding gravitational lensing data would help further to constrain the shape. Indeed elongation strongly enters in the lensing properties of a halo. Therefore gravitational lensing features brings information on the elongation of the total matter distribution.

Mahdavi et al. (2007) provided a framework for the joint analysis of cluster observations (JACO) which fits the mass models simultaneously to X-ray, SZ, and weak lensing data. They applied this method to Abell 478, assuming *spherical symmetry*. They do find a good agreement between all data sets, which points out that the spherical symmetry hypothesis was well motivated in the case of Abell 478.

However, we stress that it can be questionable to combine different data sets assuming spherical symmetry: if a given galaxy cluster exhibits a significant mass discrepancy between X-ray and lensing estimates assuming spherical symmetry, then a simultaneous fit of both data sets using a spherical model is not appropriate.

The non parametric method based on Abel's integral discussed in the previous Section has been applied to some clusters in order to study the temperature and density profiles of the ICM, assuming *spherical symmetry*: Yuan et al. (2008) and Kitayama et al. (2004) for RXJ 1347; Nord et al. (2009) for Abell 2163; and Basu et al. (2010) for Abell 2204.

Recently, Mahdavi and Chang (2011) derived a model-independent expression for the minimum line of sight extent of the hot plasma in a cluster of galaxies. No a priori assumptions regarding equilibrium or geometry are required, and the inputs are X-ray and SZ data. They applied this method to the Bullet Cluster, and constrained a *minimum* line of sight / plane of the sky axial ratio of ~ 1 .

In deprojecting, assumptions regarding the three-dimensional structure of the DM or the ICM are often required, as well as the assumption regarding hydrostatic equilibrium. Although these assumptions could be justified in relaxed and uni-modal clusters (i.e. clusters for which the mass distribution can be described using a single mass clump), they are likely to be too strong for the vast majority of the systems. Indeed, numerical simulations often show that clusters deviate systematically from hydrostatic equilibrium, especially at large radii ($R > R_{500}$). The main interpretation for this result is that clusters, being relatively young structures, are dynamically active and continue to accrete mass from their outskirts. Bulk motions of the gas lead to non-thermal pressure support and thus alter the state of hydrostatic equilibrium (Piffaretti and Valdarnini 2008; Lau et al. 2009). In fact, as shown by Rasia et al. (2006), X-ray mass estimates of simulated clusters based on the hydrostatic equilibrium assumptions are biased low by 10 – 15%. The bias is however dependent on the gas physics implemented in the simulation. For example, Rasia et al. (2012) find that the bias is sensitive to the model assumed to include thermal conduction in hydrodynamical simulations. Observational results by the CCCP and the LoCuss collaborations (e.g. Mahdavi et al. 2008; Zhang et al. 2010), based on the comparison between X-ray and lensing masses of large samples of clusters, seem to support the view emerging from the simulations: if we believe that the lensing masses are nearly un-biased on average (Meneghetti et al. 2010a), the ratio between X-ray and lensing masses should give an indication of the lack of hydrostatic equilibrium in these systems. From the above mentioned observational projects, it emerges that X-ray masses are generally smaller than the lensing masses by $\sim 15\%$.

3 Priors

Besides combining different observational data sets and performing a simultaneous fit of a triaxial mass model, it is also possible to consider well motivated priors in order to narrow down the parameter space that will be explored when performing the fit. We refer the reader to Corless and King (2008) and Corless et al. (2009) for a thorough discussion. Use of priors applies when the fit is performed on a single given data set or when the fit is applied to complementary data sets. Of course, the fewer data sets one is using and/or the poorer the quality of these data sets, the more one relies on priors. Priors sometimes rely on the results from N-body simulations which reasonably capture the physics of the DM, being dominated by the gravity and hence relatively simple. However, predictions are coming from dissipationless N-body simulations, and the physics of baryons may modify predictions, specially in the inner part of galaxy clusters where most of the baryons are found.

For example, Corless and King (2008) presented a Bayesian MCMC (Monte Carlo Markov Chain) method to fit fully triaxial NFW haloes to weak lensing data. Their method allows to combine weak lensing data with prior probability functions on the model haloe parameters to return parameter and error estimates that reflect the true uncertainties of the problem.

A similar approach has been proposed by Mauro Sereno and collaborators (Sereno and Umetsu 2011; Sereno and Zitrin 2012). Using weak and strong lensing data sets, they deprojected the surface density maps to infer the triaxial structure of the cluster. Priors were propagated through the inversion by means of the Bayes theorem. The method proceeds as follows. As a first step, they obtain the surface mass density of a galaxy cluster by strong-lensing modelling of multiple images or/and weak lensing analysis of shear and magnification. As a second step, a projected ellipsoidal NFW haloe with arbitrary orientation is fitted to the convergence map. Finally, the measured distributions of projected parameters are recovered using Bayesian statistics.

Given the measured convergence map k_{obs} , the weak lensing χ_{WL}^2 function can be expressed as (Oguri et al. 2005),

$$\chi_{\text{WL}}^2 = \sum_{i,j} [k_{\text{obs}}(\mathbf{r}_i) - \mathbf{k}(\mathbf{r}_i)] (V^{-1})_{i,j} [k_{\text{obs}}(\mathbf{r}_j) - \mathbf{k}(\mathbf{r}_j)] \quad (5)$$

where \mathbf{V}^{-1} is the inverse of the pixel-pixel covariance matrix. The corresponding likelihood is $\mathcal{L}_{\text{WL}} \propto \exp(-\chi_{\text{WL}}^2/2)$.

As far as strong lensing is concerned, one can use either a parametric or a non-parametric approach in order to retrieve the surface mass density map.

The final likelihood to be employed in the Bayes' theorem is then $\mathcal{L}(\kappa_s, r_{\text{SP}}, \epsilon, \theta_\epsilon)$, where $\kappa_s, r_{\text{SP}}, \epsilon, \theta_\epsilon$ corresponds to the lensing strength, the projected length scale, the projected ellipticity and the ellipticity in the plane of the sky of an ellipsoidal NFW haloe respectively. Each projected parameter is on turn a function of the intrinsic shape and orientation. According to the relevant data-set, the likelihood is \mathcal{L}_{WL} , \mathcal{L}_{SL} or $\mathcal{L}_{\text{All}} \propto \mathcal{L}_{\text{WL}} \times \mathcal{L}_{\text{SL}}$ for weak, strong or combined strong plus weak lensing analyses, respectively.

We emphasise that strong lensing clusters are typically more elliptical in the core than in the weak lensing probed region (see, *e.g.* Meneghetti et al. 2010a). This may have important consequences when the likelihoods are combined.

3.1 Priors on the Axis Ratio

Using a spherical mass model is equivalent to putting δ -function priors on both axis ratios, which is a strong prior. The opposite would be to impose a weak flat prior on both axis ratios.

A prior on the axis ratio of a triaxial model has been used in recent works by Mauro Sereno and collaborators. It is detailed below. We note that Oguri et al. (2005) were the first to use this prior.

The distribution of minor to major axis ratios ($\eta_{\text{DM},a}$) can be approximated as (Jing and Suto 2002; Lee et al. 2005),

$$p(\eta_{\text{DM},a}) \propto \exp \left[-\frac{(\eta_{\text{DM},a} - \eta_\mu/r)^2}{2\sigma_s^2} \right] \quad (6)$$

where the parameters of these distributions were obtained from numerical simulations: $\eta_\mu = 0.54$, $\sigma_s = 0.113$ and

$$r = (M_{\text{vir}}/M_*)^{0.07\Omega_M(z)^{0.7}}, \quad (7)$$

with M_* the characteristic nonlinear mass at redshift z and M_{vir} the virial mass.

The conditional probability for intermediate to major axis ratio $\eta_{\text{DM},b}$ goes as

$$p(\eta_{\text{DM},a}/\eta_{\text{DM},b}|\eta_{\text{DM},a}) = \frac{3}{2(1-r_{\text{min}})} \left[1 - \frac{2\eta_{\text{DM},a}/\eta_{\text{DM},b} - 1 - r_{\text{min}}}{1 - r_{\text{min}}} \right] \quad (8)$$

for $\eta_{\text{DM},a}/\eta_{\text{DM},b} \geq r_{\text{min}} \equiv \max[\eta_{\text{DM},a}, 0.5]$, whereas is null otherwise. The distribution of axial ratios of the lensing population mimics that of the total cluster population (Hennawi et al. 2007).

As prior for the intrinsic shape, we consider a flat distribution for the axial ratios in the range $\eta_{\text{min}} < \eta_{\text{DM},a} \leq 1$ and $\eta_{\text{DM},a} \leq \eta_{\text{DM},b} \leq 1$. Probabilities are defined such that the marginalised probability $P(\eta_{\text{DM},a})$ and the conditional probability $P(\eta_{\text{DM},b}|\eta_{\text{DM},a})$ are constant. The probabilities can then be expressed as

$$p(\eta_{\text{DM},a}) = 1/(1 - \eta_{\text{min}}) \quad (9)$$

for the full range $\eta_{\text{min}} < \eta_{\text{DM},a} \leq 1$ and

$$p(\eta_{\text{DM},b}|\eta_{\text{DM},a}) = (1 - \eta_{\text{DM},a})^{-1} \quad (10)$$

for $\eta_{\text{DM},b} \geq \eta_{\text{DM},a}$ and zero otherwise. The resulting probability for $\eta_{\text{DM},b}$ is then

$$p(\eta_{\text{DM},b}) = \frac{1}{1 - \eta_{\text{min}}} \ln \left(\frac{1 - \eta_{\text{min}}}{1 - \eta_{\text{DM},b}} \right). \quad (11)$$

A flat distribution allows also for very triaxial clusters ($\eta_{\text{DM},a} \leq \eta_{\text{DM},b} \ll 1$), which are preferentially excluded by N -body simulations. Therefore, η_{min} is fixed to 0.1.

3.2 Strong Lensing Clusters

Different authors, based on simulations (Hennawi et al. 2007; Corless and King 2007; Oguri and Blandford 2009; Meneghetti et al. 2010a), investigated to which degree strong lensing (SL) clusters constitute a biased population of galaxy clusters. Hennawi et al. (2007) found that strong lensing clusters have 3D concentrations 18% higher than the typical cluster with similar mass. Besides, strong lensing clusters are found to be triaxial and viewed preferentially along their major axis. Therefore, we expect an additional bias to exist in the distribution of 2D concentrations (the quantity to which lensing is sensitive to). Indeed, Hennawi et al. (2007) found that they have 2D concentrations which are 34% higher than the typical cluster. The bias in concentration of strong lensing clusters may be even higher than the 18% found by Hennawi et al. (2007). Meneghetti et al. (2010a) showed that the strongest gravitational lenses (i.e. characterised by large lensing cross sections) are typically affected by much larger concentration bias (up to 100%). The bias also depends on the cluster redshift, being stronger at those redshifts that are least favourable for strong lensing. Indeed, at these redshifts, only clusters very elongated along the line of sight seem able to produce strong lensing events.

It is now well established that strong lensing clusters constitute a biased population of triaxial haloes whose major axis is preferentially aligned with the line of sight, boosting the lensing efficiency. Therefore, when studying galaxy clusters presenting strong lensing features, using a prior on the angle between its major axis and the line

of sight is reasonable and has been used in a number of studies (*e.g.* Corless et al. 2009; Sereno and Umetsu 2011; Sereno and Zitrin 2012).

If θ represents the angle between the major axis of the halo and our line of sight, this orientation bias can be expressed as:

$$p(\cos\theta) \propto \exp\left[-\frac{(\cos\theta - 1)^2}{2\sigma_\theta^2}\right]. \quad (12)$$

A value of $\sigma_\theta = 0.115$ can be representative of the orientation bias for massive strong lensing clusters (Corless et al. 2009).

Apart from this strong orientation bias, it is worth noting that strong lensing clusters do not exhibit a significant excess of triaxiality and display nearly the same distribution of axis ratios as the total cluster population (Hennawi et al. 2007; Meneghetti et al. 2010a).

Having mentioned the existence of this orientation bias, it is worth noting that SL clusters do not constitute an homogeneous population: all SL clusters are not triaxial haloes with their

major axes pointing right at us. Actually, observing deep enough at any X-ray luminous cluster, it is very likely that SL features will be detected. As mentioned by Meneghetti et al. (2010a), the orientation bias is a growing function of the lensing cross section. Large Einstein radii clusters will tend to be more biased in their orientation compared to smaller Einstein radii clusters. For example, in the sample of 7 strong lensing clusters studied by Newman et al. (2012a), only 1 appears to present an orientation bias. These clusters have Einstein radii of order $\sim 20''$.

Another way to 'boost' the lensing efficiency is through merger. Indeed, mergers provide an efficient mechanism to substantially increase the strong lensing efficiency of individual clusters (Zitrin et al. 2012; Redlich et al. 2012). Therefore, both merging and elongated clusters along the line of sight are overrepresented in strong lensing cluster samples. In most cases, the optical properties should be able to disentangle both populations.

3.3 Priors from the Mass-Concentration Relation

N -body simulations (Oguri and Blandford 2009; Macciò et al. 2008; Gao et al. 2008; Duffy et al. 2008; Prada et al. 2012) have provided a picture of the expected properties of dark matter haloes. Results may depend on parameters such as the overall normalisation of the power spectrum, the mass resolution, and the simulation volume. The dependence of halo concentration on mass and redshift can be adequately described by a power law,

$$c = A(M/M_{\text{pivot}})^B (1+z)^C. \quad (13)$$

As reference, we follow Duffy et al. (2008), who used the cosmological parameters from WMAP5 and found $\{A, B, C\} = \{5.71 \pm 0.12, -0.084 \pm 0.006, -0.47 \pm 0.04\}$ for a pivotal mass $M_{\text{pivot}} = 2 \times 10^{12} M_\odot/h$ in the redshift range 0–2 for their full sample of clusters. The scatter in the concentration about the median $c(M)$ relation is lognormal,

$$p(\ln c|M) = \frac{1}{\sigma\sqrt{2\pi}} \exp\left[-\frac{1}{2}\left(\frac{\ln c - \ln c(M)}{\sigma}\right)^2\right], \quad (14)$$

with a dispersion $\sigma(\log_{10} c_{200}) = 0.15$ for a full sample of clusters (Duffy et al. 2008). Recently, Prada et al. (2012) claimed that the dependence of concentration on halo mass and its evolution can be obtained from the root-mean-square fluctuation amplitude of the linear density field. They noticed a flattening and upturn of the relation with increasing mass and estimated concentrations for galaxy clusters substantially larger than results reported in Eq. (13). However, more recently, Ludlow et al. (2012) studied how the dynamical state of dark matter haloes affects the relation between mass and concentration. When considering only dynamically relaxed haloes, they find that the aforementioned upturn disappears. Finally, Meneghetti & Rasia (submitted) show that the high amplitude and the upturn of the Prada et al. (2012) mass-concentration relation can be explained in terms of: i) the different method (compared to other works in the literature) to measure the concentration (from the measured circular velocity) and ii) the different selection applied to haloes for building the mass-concentration relation (clusters are selected by maximum circular velocity).

In the literature, there is no consensus on the evolution of the $c(M)$ relation with redshift, in particular for massive haloes. While several authors predict a strong redshift evolution of the concentrations at all mass scales (see, *e.g.* Bullock et al. 2001; Eke et al. 2001), Zhao et al. (2003) find that the evolution of the concentration of individual haloes is not just a function of redshift but is tightly connected to their mass growth rate (see also Wechsler et al. 2002). In particular, the faster the mass grows, the slower the concentration increases. Since most of the massive haloes are in a fast mass accretion phase at high redshift, they find that the cluster $c(M)$ relation has a very slow redshift evolution. Similar results were found recently by Muñoz-Cuartas et al. (2011), who confirm that the growth rate of the concentration depends on the halo mass, with low-mass haloes experiencing a faster concentration evolution. These authors also find that the evolution of the $c(M)$ relation is faster at lower redshifts than at higher redshifts.

3.4 On the Choice of Priors

The choice of priors used on the parameters of a triaxial model is very important because of the inherently under-constrained nature of the problem. This choice should be carefully made with respect to the particular problem at hand. For example, if one wants to test the mass-concentration relation predicted by the Λ CDM scenario, adopting a prior based on that relation would not be relevant. On the other hand, if one aims to model a sample of dark matter haloes to calculate a mass function, a loose mass-concentration prior may be appropriate in order to take into account existing knowledge of the cluster and group population into the model. The work by Corless et al. (2009) further illustrates this point: their weak lensing analysis of Abell 2204 is able to constrain the ellipticity in the plane of the sky, which is found to be slightly larger than what is found statistically in Λ CDM simulations. Therefore, imposing a prior on the axis ratio derived from simulations for this cluster suppresses real information and is not appropriate. This highlights the fact that a prior may be well adapted to determine the statistics of a large population of dark matter haloes, but it may not be relevant for an individual cluster.

When considering priors within a Bayesian framework, one can compute the Bayesian evidence with or without the prior and see which hypothesis performs better. It is worth noting that, the better the data, the lesser the impact of priors in Bayesian methods.

4 Three-Dimensional Structure of Galaxy Clusters: Triaxiality

We present in this Section a general parametric framework intended to simultaneously fit X-ray, SZ, and gravitational lensing (both weak and strong) data sets. It is based on the works published by Andrea Morandi and collaborators. More detail can be found in the relevant publications (Morandi et al. 2010, 2011a, 2011b; Morandi and Limousin 2012; Morandi et al. 2012b).

The lensing effects and the X-ray/SZ emission both depend on the properties of the DM gravitational potential well, the former being a direct probe of the two-dimensional mass map via the lensing equation and the latter an indirect proxy of the three-dimensional mass profile through the hydrostatic equilibrium (HE) equation applied to the gas temperature and density. In order to infer the model parameters of both the IC gas and of the underlying DM density profile, we perform a joint analysis of lensing and X-ray/SZ data. We briefly outline the methodology in order to infer physical properties in triaxial galaxy clusters:

- We start with a generalised Navarro, Frenk and White (gNFW) triaxial model of the DM as described in Jing and Suto (2002), which is representative of the total underlying mass distribution and depends on a few parameters to be determined, namely the concentration parameter c_{200} , the scale radius R_s , the inner slope of the DM γ , the two axis ratios ($\eta_{DM,a}$ and $\eta_{DM,b}$) and the Euler angles ψ , θ and ϕ
- following Lee and Suto (2003, 2004), we recover the gravitational potential and two-dimensional surface mass Σ (Equation 32) of a dark halo with such triaxial density profile
- we solve the generalised HE equation, i.e. including the non-thermal pressure P_{nt} (Equation 26), for the density of the IC gas sitting in the gravitational potential well previously calculated, in order to infer the theoretical three-dimensional temperature profile T
- we calculate the SZ temperature decrement map $\Delta T(\nu)$ (Equation 30) and the surface brightness map S_X (Equation 29) related to the triaxial ICM halo
- the joint comparisons of T with the observed temperature, of S_X with the observed brightness image, of $\Delta T(\nu)$ with the observed SZ temperature decrement, and of Σ with the observed two-dimensional mass map give us the parameters of the triaxial ICM and DM density model.

4.1 ICM & DM Triaxial Haloes

We describe the DM and ICM as ellipsoids oriented in an arbitrary direction on the sky. We introduce two Cartesian coordinate systems, $\mathbf{x} = (x, y, z)$ and $\mathbf{x}' = (x', y', z')$, which represent respectively the principal coordinate system of the triaxial dark halo and the observer's coordinate system, with the origins set at the centre of the halo. We assume that the z' -axis points along the line of sight direction of the observer and that the x', y' axes identify the directions of West and North, respectively, on the plane of the sky. We also assume that the x, y, z -axes point along the minor, intermediate and major axes, respectively, of the DM halo. We define ψ , θ and ϕ as the rotation angles about the x , y and z axis, respectively (see Figure 1). Then the relation between the two coordinate systems can be expressed in terms of the rotation matrix M as

$$\mathbf{x}' = M\mathbf{x}, \quad (15)$$

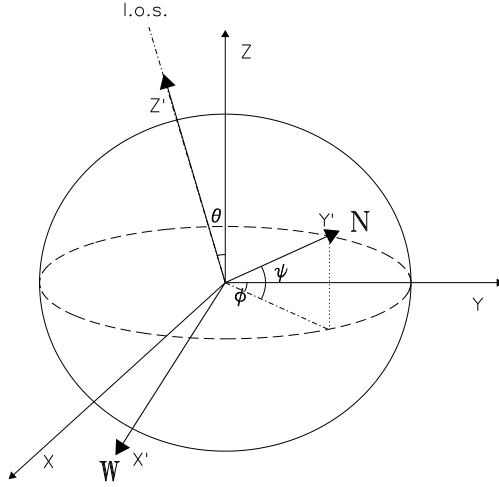


Fig. 1 The orientations of the coordinate systems. The Cartesian axes (x, y, z) represent the DM and ICM halo principal coordinate system while the axes (x', y', z') represent the observer's coordinate system with the z' -axis aligned with the line of sight (l.o.s.) direction. We define ψ , θ and ϕ as the rotation angles about the x , y and z axes, respectively. The labels **N** and **W** indicate the position of the North and West, respectively, on the plane of the sky.

where $\#$ denotes matrix multiplication and M represents the orthogonal matrix corresponding to counter-clockwise/right-handed rotations $M_x(\psi)$, $M_y(\theta)$, $M_z(\phi)$ with Euler angles ψ , θ , ϕ , and it is given by:

$$M = M_x(\psi)\#M_y(\theta)\#M_z(\phi), \quad (16)$$

where

$$M_x(\psi) = \begin{bmatrix} 1 & 0 & 0 \\ 0 & \cos \psi & -\sin \psi \\ 0 & \sin \psi & \cos \psi \end{bmatrix}; \quad (17)$$

$$M_y(\theta) = \begin{bmatrix} \cos \theta & 0 & \sin \theta \\ 0 & 1 & 0 \\ -\sin \theta & 0 & \cos \theta \end{bmatrix}; \quad (18)$$

$$M_z(\phi) = \begin{bmatrix} \cos \phi & -\sin \phi & 0 \\ \sin \phi & \cos \phi & 0 \\ 0 & 0 & 1 \end{bmatrix}. \quad (19)$$

Figure 1 represents the relative orientation between the observer's coordinate system and the halo principal coordinate system.

In order to parametrise the cluster mass distribution, we consider a triaxial generalised Navarro, Frenk & White model (gNFW, *e.g.* Jing and Suto 2002):

$$\rho(R) = \frac{\delta_c \rho_{c,z}}{(R/R_s)^\gamma (1 + R/R_s)^{3-\gamma}}, \quad (20)$$

where R_s is the scale radius, δ_c is the dimensionless characteristic density contrast with respect to the critical density of the Universe $\rho_{c,z}$ at the redshift z of the cluster, and γ represents the inner slope of the density profile; $\rho_{c,z} \equiv 3H(z)^2/8\pi G$ is the critical density of the universe at redshift z , $H_z \equiv E_z H_0$, $E_z = [\Omega_M(1+z)^3 + \Omega_\Lambda]^{1/2}$, and

$$\delta_c = \frac{200}{3} \frac{c_{200}^3}{F(c_{200}, \gamma)}, \quad (21)$$

where $c_{200} \equiv R_{200}/R_s$ is the concentration parameter, with (Wyithe et al. 2001):

$$F(y, \gamma) \equiv \int_0^y s^{2-\gamma}(1+s)^{\gamma-3} ds. \quad (22)$$

The radius R can be regarded as the major axis length of the iso-density surfaces:

$$R^2 = c^2 \left(\frac{x^2}{a^2} + \frac{y^2}{b^2} + \frac{z^2}{c^2} \right), \quad (a \leq b \leq c). \quad (23)$$

We have previously defined $\eta_{\text{DM},a} = a/c$ and $\eta_{\text{DM},b} = b/c$ as the minor-major and intermediate-major axis ratios of the DM haloe, respectively.

The gravitational potential of a dark haloe with the triaxial density profile (Equation 20) can be written in terms of complex implicit integrals (Binney and Tremaine 1987). While numerical integration is required in general to obtain the triaxial gravitational potential, Lee and Suto (2003) retrieved the following approximation (which holds for small eccentricities for the gravitational potential Φ under the assumption of triaxial gNFW model for the DM (Equation 20):

$$\Phi(\mathbf{u}) \simeq C_0 F_1(u) + C_0 \frac{e_b^2 + e_c^2}{2} F_2(u) + C_0 \frac{e_b^2 \sin^2 \theta \sin^2 \phi + e_c^2 \cos^2 \theta}{2} F_3(u), \quad (24)$$

with $\mathbf{u} \equiv \mathbf{r}/R_s$, $C_0 = 4\pi G \delta_c \rho_c(z) R_s^2$, and the three functions, $F_1(u)$, $F_2(u)$, and $F_3(u)$ have been defined in Morandi et al. (2010), e_b (ϵ_b) and e_c (ϵ_c) are the eccentricity of DM (IC gas) with respect to the major axis (e.g. $e_b = \sqrt{1 - (b/c)^2}$).

The work of Lee and Suto (2003) showed that the iso-potential surfaces of the triaxial dark haloe are well approximated by a sequence of concentric triaxial distributions of radius R_{icm} with different eccentricity ratio. For R_{icm} a similar definition as for R holds (Equation 23), but with eccentricities ϵ_b and ϵ_c . Note that $\epsilon_b = \epsilon_b(e_b, u, \gamma)$ and $\epsilon_c = \epsilon_c(e_c, u, \gamma)$, unlike the constant e_b, e_c for the adopted DM haloe profile. In the whole range of u , ϵ_b/e_b (ϵ_c/e_c) is less than unity (~ 0.7 at the centre), i.e., the intracluster gas is altogether more spherical than the underlying DM haloe (see Morandi et al. (2010) for further details).

The iso-potential surfaces of the triaxial dark haloe coincide also with the iso-density (pressure, temperature) surfaces of the intracluster gas. This is simply a direct consequence of the *X-ray shape theorem* (Buote and Canizares 1994); the HE equation (26) yields

$$\nabla P \times \nabla \Phi = \nabla \rho_{\text{gas}} \times \nabla \Phi = 0. \quad (25)$$

4.2 X-ray, SZ and lensing equations

For the X-ray analysis we rely on a generalisation of the HE equation (Morandi et al. 2011b), which accounts for the non-thermal pressure P_{nt} and reads:

$$\nabla P_{\text{tot}} = -\rho_{\text{gas}} \nabla \Phi \quad (26)$$

where ρ_{gas} is the gas mass density, Φ is the gravitational potential, $P_{\text{tot}} = P_{\text{th}} + P_{\text{nt}}$. We implemented a model where P_{nt} is a fraction of the total pressure P_{tot} , and we set this fraction to be a power law with the radius (Shaw et al. 2010):

$$\frac{P_{\text{nt}}}{P_{\text{tot}}} = \xi (R/R_{200})^n . \quad (27)$$

Note that X-ray data probe only the thermal component of the gas $P_{\text{th}} = n_e \mathbf{k}T$, \mathbf{k} being the Boltzmann constant. From Equations (26) and (27) we point out that neglecting P_{nt} (i.e. $P_{\text{tot}} = P_{\text{th}}$) systematically biases low the determination of cluster mass profiles. This effect increases at larger radii, where the contribution of the gas motion is larger.

Given that Equation (26) is a first order differential equation, we need a boundary condition on the pressure, \tilde{P} , which represents the pressure at R_{200} , and it is an unknown parameter to be determined.

To model the electron density profile in the triaxial ICM haloe, we use the following fitting function, which corresponds to a simplified version of the function given by Vikhlinin et al. (2006a):

$$n_e(R_{\text{icm}}) = n_0 (R_{\text{icm}}/r_{c_1})^{-\delta} (1 + R_{\text{icm}}^2/r_{c_1}^2)^{-3/2\varepsilon + \delta/2} (1 + R_{\text{icm}}^4/r_{c_2}^4)^{-\nu/4} \quad (28)$$

with parameters $(n_0, r_{c_1}, \varepsilon, \delta, r_{c_2}, \nu)$. We computed the theoretical three-dimensional temperature T by numerically integrating the equation of the HE (Equation 26), assuming triaxial geometry and a functional form of the gas density given by Equation (28).

The observed X-Ray surface brightness S_X is given by:

$$S_X = \frac{1}{4\pi(1+z)^4} \Lambda(T_{\text{proj}}^*, Z) \int n_e n_p dz' , \quad (29)$$

where $\Lambda(T_{\text{proj}}^*, Z)$ is the cooling function. Since the projection on the sky of the plasma emissivity gives the X-ray surface brightness, the latter can be geometrically fitted with the model $n_e(R_{\text{icm}})$ of the assumed distribution of the electron density (Equation 28) by applying Equation (29). This has been accomplished via simulated *Chandra* spectra, where the current model is folded through response curves (ARF and RMF) and then added to a background file, and with absorption, temperature and metallicity measured in that neighbouring ring in the spectral analysis. In order to calculate $\Lambda(T_{\text{proj}}^*, Z)$, we adopted a MEKAL model for the emissivity.

The thermal SZ effect is expressed as a small variation in the temperature $\Delta T(\nu)$ of the CMB as a function of the observation frequency:

$$\frac{\Delta T(\nu)}{T_{\text{cmb}}} = \frac{\sigma_T}{m_e c^2} \int P_e(\mathbf{r}) f(\nu; T(\mathbf{r})) dz' \quad (30)$$

where σ_T is the Thomson cross-section, $P_e(\mathbf{r}) \equiv n_e(\mathbf{r}) \mathbf{k} T_e(\mathbf{r})$ is the pressure of the electrons of the ICM at the volume element of coordinate \mathbf{r} , \mathbf{k} is the Boltzmann constant, and $T_{\text{cmb}} = 2.725$ K.

$f(\nu; T(\mathbf{r}))$ takes into account the spectral shape of the SZ effect and it reads:

$$f(\nu; T(\mathbf{r})) = \left(x \frac{e^x + 1}{e^x - 1} - 4 \right) (1 + o_f(x; T)), \quad (31)$$

where $x = h\nu/kT_{\text{cmb}}$ accounts for the frequency dependence of the SZ effect, and for the relativistic corrections related to the term $o_f(x, T)$ (Itoh et al. 1998). Note that in Equation (30) we account for the implicit dependence of $f(\nu; T(\mathbf{r}))$ on the radius.

Next, the two-dimensional SZ model $\Delta T(\nu)$ is convolved with the instrumental point-spread function and the measured transfer function. In practise, the transfer function convolution is performed via multiplication in the Fourier domain. This filtering significantly reduces the peak decrement of the cluster and creates a ring of positive flux at $r \sim 2$ arcmin. This filtered model is then compared to the observed SZ temperature decrement map. We also calculated the noise covariance matrix \mathbf{C} among all the pixels of the observed SZ temperature decrement map through 1000 jackknife realisations of our cluster noise. In this perspective we assumed that the noise covariance matrix for SZ data is diagonal, as this was shown to be a good assumption in Sayers et al. (2011a).

For the lensing analysis the two-dimensional surface mass density Σ can be expressed as:

$$\Sigma = \int_{-\infty}^{\infty} \rho(R) dz' \quad (32)$$

We also calculated the covariance matrix \mathbf{C} among all the pixels of the reconstructed surface mass (see Morandi et al. (2011b) for further details).

4.3 Joint X-ray+SZ+Lensing Analysis

The probability distribution function of model parameters has been evaluated via Markov Chain Monte Carlo (MCMC) algorithm, by using as proposal density a likelihood \mathcal{L} and a standard method for rejecting proposed moves. This allows to compare observations and predictions, and to infer the desired physical parameters. The likelihood has been constructed by performing a joint analysis for lensing and X-ray/SZ data. More specifically, the system of equations we simultaneously rely on in our joint X-ray + SZ + lensing analysis is:

$$\begin{aligned} & T(c_{200}, R_s, \gamma, \eta_{\text{DM},a}, \eta_{\text{DM},b}, \psi, \theta, \phi, n_0, r_{c_1}, \varepsilon, \delta, r_{c_2}, \nu, \xi, n, \tilde{P}) \\ & S_X(c_{200}, R_s, \gamma, \eta_{\text{DM},a}, \eta_{\text{DM},b}, \psi, \theta, \phi, n_0, r_{c_1}, \varepsilon, \delta, r_{c_2}, \nu) \\ & \Delta T(c_{200}, R_s, \gamma, \eta_{\text{DM},a}, \eta_{\text{DM},b}, \psi, \theta, \phi, n_0, r_{c_1}, \varepsilon, \delta, r_{c_2}, \nu, \xi, n, \tilde{P}) \\ & \Sigma(c_{200}, R_s, \gamma, \eta_{\text{DM},a}, \eta_{\text{DM},b}, \psi, \theta, \phi) \end{aligned} \quad (33)$$

where the parameters c_{200} (concentration parameter), R_s (scale radius), γ (inner DM slope), $\eta_{\text{DM},a}$ (minor-major axis ratio), $\eta_{\text{DM},b}$ (intermediate-major axis ratio), and ψ, θ, ϕ (Euler angles) refer to the triaxial DM haloe (Equation 20); the parameters $n_0, r_{c_1}, \varepsilon, \delta, r_{c_2}, \nu$ refer to the IC gas density (Equation 28); ξ, n (normalisation and

slope, respectively) refer to the non-thermal pressure (Equation 27); and \tilde{P} to the pressure at R_{200} , which is a boundary condition of the generalised HE equation (Equation 26).

In this triaxial joint analysis the three-dimensional model temperature T is recovered by solving equation (26) and constrained by the observed temperature profile; the surface brightness is recovered via projection of the gas density model (Equation 29) and constrained by the observed brightness; the SZ signal is deduced via projection of the three-dimensional pressure (Equation 30) and constrained by the observed SZ temperature decrement; and the model two-dimensional mass density Σ is recovered via Equation (32) and constrained by the observed surface mass density.

Hence the likelihood $\mathcal{L} \propto \exp(-\chi^2/2)$, and χ^2 reads:

$$\chi^2 = \chi_{x,T}^2 + \chi_{x,S}^2 + \chi_{SZ}^2 + \chi_{\text{lens}}^2 \quad (34)$$

with $\chi_{x,T}^2$, $\chi_{x,S}^2$, χ_{SZ}^2 and χ_{lens}^2 being the χ^2 coming from the X-ray temperature, X-ray brightness, SZ temperature decrement and lensing data, respectively. We note that, when both weak (lensing WL) and strong lensing (SL) data are available (Morandi et al. 2011b), $\chi_{\text{lens}}^2 = \chi_{\text{WL}}^2 + \chi_{\text{SL}}^2$.

For the spectral analysis, $\chi_{x,T}^2$ is equal to:

$$\chi_{x,T}^2 = \sum_{i=1}^{n^*} \frac{(T_{\text{proj},i} - T_{\text{proj},i}^*)^2}{\sigma_{T_{\text{proj},i}}^2} \quad (35)$$

$T_{\text{proj},i}^*$ being the observed projected temperature profile in the i th circular ring and $T_{\text{proj},i}$ the azimuthally-averaged projection (following Mazzotta et al. 2004) of the theoretical three-dimensional temperature T ; the latter is the result of solving the HE equation, with the gas density $n_e(R_{\text{icm}})$.

For the X-ray brightness, $\chi_{x,S}^2$ reads:

$$\chi_{x,S}^2 = \sum_j \sum_{i=1}^{N_j} \frac{(S_{X,i} - S_{X,i}^*)^2}{\sigma_{S,i}^2} \quad (36)$$

with $S_{X,i}$ and $S_{X,i}^*$ theoretical and observed counts in the i th pixel of the j th image. Given that the number of counts in each bin might be small (< 5), then we cannot assume that the Poisson distribution from which the counts are sampled has a nearly Gaussian shape. The standard deviation (i.e., the square-root of the variance) for this low-count case has been derived by Gehrels (1986):

$$\sigma_{S,i} = 1 + \sqrt{S_{X,i}^* + 0.75} \quad (37)$$

which has been proved to be accurate to approximately one percent. Note that we added background to $S_{X,i}$ as measured locally in the brightness images, and that the vignetting has been removed in the observed brightness images.

For the SZ (lensing) constraint \mathbf{D} , the $\chi_{\mathbf{D}}^2$ contribution is:

$$\chi_{\mathbf{D}}^2 = [\mathbf{D} - \mathbf{D}^*]^\dagger \mathbf{C}^{-1} [\mathbf{D} - \mathbf{D}^*], \quad (38)$$

where \mathbf{C} is the covariance matrix of the two-dimensional SZ temperature decrement (projected mass density), \mathbf{D}^* are the observed measurements of the two-dimensional

SZ temperature decrement (projected mass density) in the i th pixel, and \mathbf{D} is the theoretical 2D model.

Errors on the individual parameters have been evaluated by considering average value and standard deviation on the marginal probability distributions of the same parameters.

So we can determine the physical parameters of the cluster, for example the 3D temperature T , the shape of DM and ICM, just by relying on the generalised HE equation and on the robust results of the hydrodynamical simulations of the DM profiles. In Fig. 2 we present an example of a joint analysis for T , S_X , $\Delta T(\nu)$ and Σ : for S_X , $\Delta T(\nu)$ and Σ the 1D profile has been presented only for visualisation purpose, the fit being applied on the 2D X-ray brightness/SZ/surface mass data. Note that in the joint analysis both X-ray, SZ and lensing data are well fitted by our model, with a $\chi_{\text{red}}^2 = 1.04$.

4.4 Limitations

The BCG: The centre of galaxy clusters is usually populated by a bright central galaxy (BCG). Actually, the BCG has an influence on the formation of multiples images (Meneghetti et al. 2003; Donnarumma et al. 2011), and the physical processes taking place in the BCG substantially influence the X-ray gas (Gitti et al. 2012). In the tri-axial framework described in this Section, we have removed the central 25 kpc of the data in the joint analysis, to avoid the contamination from the BCG. However, modelling properly the BCG contribution is essential in order to probe the dark matter distribution in the very centre.

In galaxy cluster Abell 1703, the strong lensing analysis by Limousin et al. (2008) takes into account the stellar contribution of the BCG in a parametric mass modelling aimed at constraining the underlying smooth dark matter component distribution, in particular the inner slope of the dark matter distribution.

A more advanced approach which requires high quality spectroscopic data is to combine lensing observations with the stellar kinematics of the BCG (Sand et al. 2002, 2004, 2008; Newman et al. 2011, 2012a, 2012b). These studies found density profiles shallower than canonical NFW models at radii < 30 kpc, comparable to the effective radii of the BCG.

Numerical simulations by Dubinski (1998) suggested that the measured velocity dispersion profile strongly depends on the line of sight, where the central value peaks between 300 and 450 km s^{-1} depending on the considered line of sight. However, recent observations do not confirm this claim. In the sample of 7 massive strong lensing clusters studied by Newman et al. (2012a), the observed velocity profiles display a very homogeneous shape which are mutually consistent. Similar conclusions is reached within the SAURON project (Cappellari et al. 2007), which found that in giant slowly/non rotating ellipticals (including BCGs), the average shape of the velocity ellipsoid does not differ by more than ~ 10 per cent from a spherical shape.

The gas mass component: When studying the dark matter distribution, we did not subtract the mass contribution from the X-ray gas to the total mass. Nevertheless, the contribution of the gas to the total matter is small: the measured gas fraction is 0.06-0.07 in the spatial range 30-400 kpc, and the slope of the density profile is very similar to that of the DM beyond a characteristic scale ~ 20 -30 kpc, a self-similar property of

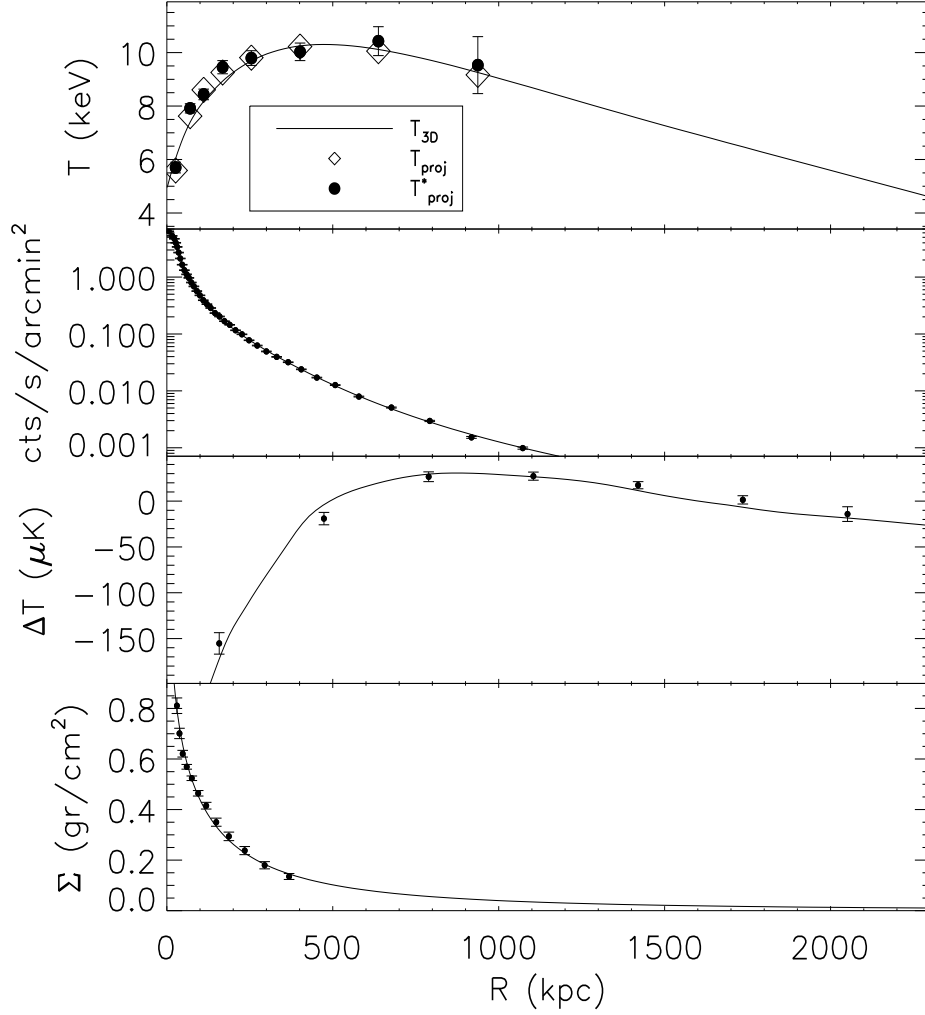


Fig. 2 Example of the joint analysis for T , S_X , $\Delta T(\nu)$ and Σ , from Morandi et al. (2012b). In the upper panel we display the two quantities which enter in the X-ray analysis (Equation 35): the observed spectral projected temperature $T_{\text{proj},m}^*$ (big points with errorbars) and the theoretical projected temperature $T_{\text{proj},m}$ (diamonds). We also show the theoretical 3D temperature (solid line), which generates $T_{\text{proj},m}$ through convenient projection techniques. In the second panel from the top we display the two quantities which enter in the X-ray brightness analysis (Equation 36): the observed surface brightness profile S_X^* (points with errorbars) and the theoretical one S_X (solid line). In the third panel from the top we display the two quantities which enter in the SZ temperature decrement analysis (Equation 30): the observed SZ temperature decrement profile (points with errorbars) and the theoretical one $\Delta T(\nu)$ (solid line). Both observed and theoretical SZ temperature decrement are convolved with the transfer function: note that this filtering significantly reduces the peak decrement of the cluster and creates a ring of positive flux at $r \sim 2$ arcmin. In the lowest panel we display the two quantities which enter in the lensing analysis (Equation (38)): the observed surface mass profile Σ^* (points with error bars) and the theoretical one Σ (solid line). Note that for surface brightness (surface mass) and the SZ data the 1D profile is presented for visualisation purpose only, the fit being applied on the 2D data. Moreover, for the surface brightness we plotted data referring to the observation ID 6880. The virial radius corresponds to a scale length on the plane of the sky of $\sim \eta_{\text{DM},a} \cdot R_{200} \approx 2240$ kpc.

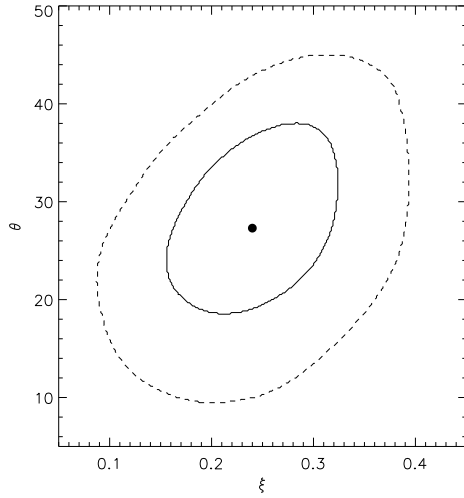


Fig. 3 Degeneracies between θ and ξ . θ represents the angle between the major axis of the halo and our line of sight, and ξ is related to the amount of non-thermal component considered in the model. The solid (dashed) line represent the 1 (2)- σ error region, while the point represents the best fit value.

the gas common to cool core clusters (Morandi and Ettori 2007), suggesting that the assumption to model the total mass as a gNFW is reliable. Similar conclusions have been reached by Bradač et al. (2008) and Sommer-Larsen and Limousin (2010).

4.5 Degeneracies & Priors

Degeneracies arise between the different parameters involved in the modelling. Fig. 3 presents the degeneracies expected between θ and ξ . θ represents the angle between the major axis of the halo and our line of sight, and ξ is related to the amount of non-thermal component considered in the model. In Fig. 4 we present the joint probability distribution among different parameters in our triaxial model for Abell 1689.

Regarding the use of priors, we point out that, when combining complementary data sets as described in this Section, we do not need to rely on any priors like those discussed in Section 3. This is welcome since priors may be potentially biased due to our incomplete understanding of cluster physics.

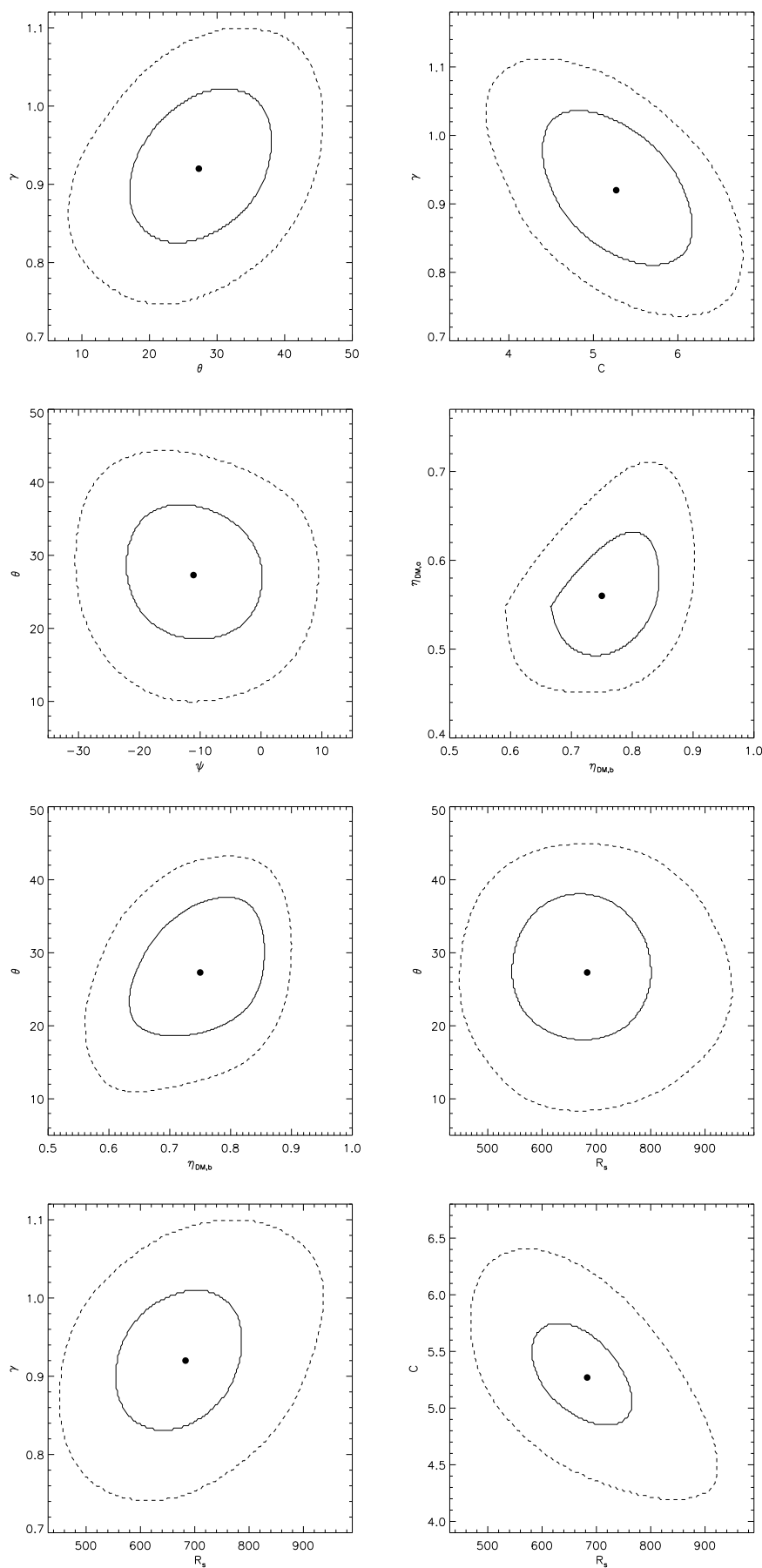


Fig. 4 Marginal probability distribution among different parameters in the triaxial model for Abell 1689 (results from Morandi et al. 2011b, but updated within the full triaxial framework presented in this Section). The solid (dashed) line represent the 1 (2)- σ error region, while the point represents the best fit value.

5 Three-Dimensional Mass Distribution in A1689 (and Other Clusters)

We aim to illustrate how spherical and triaxial modelling can lead to different halo parameters. For this purpose, we focus on galaxy cluster Abell 1689 which has been extensively studied at different wavelengths. Abell 1689 is a massive galaxy cluster at redshift 0.18 with a very large Einstein radius, around $45''$ for a source redshift ~ 2 .

Before going into detail, we would like to emphasise the complexity of this structure and try to justify why we treat such a complicated structure using a single mass clump.

Lokas et al. (2006) used spectroscopic redshifts to study the kinematics of about 200 galaxies in the cluster. They showed that the cluster is probably surrounded by a few structures aligned along the line of sight. Czoske (2004) reported redshifts for 525 galaxies, spanning from the centre outward to $3h^{-1}$ Mpc. They found only one apparently distinct group of galaxies that lies about 350 kpc to the northeast of the cluster centre. It corresponds to a group of bright galaxies well identified in optical images of this cluster. All strong lensing studies have taken into account the gravitational perturbation it generates, but its contribution to the total mass budget is found to be small. The redshift distribution of these galaxies is skewed toward slightly higher redshifts. On larger scales ($R > 1h^{-1}$ Mpc), no evidence for any substructures is found: the outskirts of Abell 1689 look rather homogeneous. However, deep X-ray observations obtained with Suzaku (Kawaharada et al. 2010) reveal anisotropic gas temperature and entropy distributions in the cluster outskirts.

If Abell 1689 appears as a complex structure, the main mass clump seems to be dominant in the mass budget: all strong lensing studies find the mass centre to coincide with the brightest cluster galaxy, which also coincides with the peak of the circular X-ray emission (Lemze et al. 2008). Besides, deep Chandra data have revealed the presence of a cool core (Riemer-Sørensen et al. 2009).

5.1 Spherical Analysis: the Abell 1689 Puzzle

While it has been proposed as a standard example of a relaxed object in hydrostatic equilibrium, Abell 1689 has been the subject of some controversies. To summarise, as long as spherical symmetry has been assumed, this cluster has been problematic in two ways:

- High concentration parameters (up to ~ 30) have been derived from lensing analyses. These large values represent a major inconsistency with the theoretical Λ CDM expectations ($c \sim 3 - 4$, Neto et al. 2007; Duffy et al. 2008).
- The 2D mass derived from X-ray data is only half of the mass found using SL estimates.

In the following, we discuss these two points and then we turn to triaxial models and how they have allowed to resolve these issues.

The concentration parameter of Abell 1689 has been constrained extensively by different authors, finding very different results. In weak lensing analyses, first studies reported $c_{200} = 4.8$ (King et al. 2002); $3.5^{+0.5}_{-0.3}$ (Bardeau et al. 2005), but these analyses likely suffered from dilution of the inner shear profile by foreground cluster members. On the other hand, very high concentrations were also inferred from weak lensing analyses based on Subaru data: $c_{200} = 30.4$ (Halkola et al. 2006); $22.1^{+2.9}_{-4.7}$ (Medezinski et al. 2007). Using the same Subaru data but a different algorithm, other

authors reported a smaller concentration parameter, between 10 and 15 (Umetsu et al. 2009, 2011). Weak and strong lensing analyses converged to: $c_{200}=7.9$ (Clowe 2003); $7.6^{+0.3}_{-0.5}$ (Halkola et al. 2006); 7.6 ± 1.6 (Limousin et al. 2007), values which are still high compared to the theoretical expectations. Actually, only a few haloes formed in the Millennium simulation could reach this value (Neto et al. 2007). These values were found in agreement with X-ray analyses: $c_{200} = 7.7^{+1.7}_{-2.6}$ (Andersson and Madejski 2004); 6.6 ± 0.4 (Peng et al. 2009).

Besides the large variance in the concentration parameter, these studies agree on the fact that the mass derived from X-ray measurement is half of that found from strong gravitational lensing at most radii (see also Lemze et al. 2008).

Riemer-Sørensen et al. (2009) showed that this discrepancy is reduced if we exclude a cool clump plus some substructure in the North-Eastern part of the cluster; nevertheless a discrepancy still remains in the strong lensing region.

A way to reconcile the mass derived from X-ray and lensing measurement within a spherical mass distribution is to add the contribution from non-thermal pressure. In the case of Abell 1689, Molnar et al. (2010) found a contribution of about 40%. This is larger than the theoretical expectations by (Shaw et al. 2010) but consistent with the set of simulations by Molnar et al. (2010).

5.2 Triaxial Models: Solving the Puzzle

Oguri et al. (2005), using a triaxial mass model, found that weak lensing measurements in Abell 1689 based on Subaru data are indeed compatible with Λ CDM if Abell 1689 represents a rare population ($\sim 6\%$ by number) of cluster-scale haloes. Corless et al. (2009) constrained the triaxial shape of the total mass distribution of Abell 1689 via weak lensing data and under a range of Bayesian priors derived from theory, though large errors accompany their triaxial parameter estimates.

Morandi et al. (2011a) presented the determination of the intrinsic shapes and the physical parameters of both DM and ICM in Abell 1689 by combining X-ray and strong lensing data. They showed that Abell 1689 can be described as elongated along the line of sight, with a minor-major principal axis ratio equal to 0.42 ± 0.02 . They assumed that the triaxial ellipsoid is oriented along the line of sight, an assumption justified in light of the "orientation bias" of strong lensing clusters (see Section 3.2). A subsequent re-analysis of Morandi et al. (2011b), by jointly analysing also weak lensing data and accounting for the non-thermal pressure of the IC gas, strengthened the view of a triaxial cluster elongated along the line of sight, though a bit larger value of the minor-major principal axis ratio has been inferred (0.50 ± 0.01). Besides, it was shown in this work that the large Einstein radius observed was reproduced by a triaxial model with Λ CDM friendly parameters. In the present review we extend these previous works, by allowing the DM and ICM ellipsoids to be oriented in an arbitrary direction on the sky (see Section 4 for further details). Our work indicates that Abell 1689 is a triaxial galaxy cluster with DM halo axial ratios $\eta_{DM,a} = 0.56 \pm 0.07$ and $\eta_{DM,b} = 0.75 \pm 0.08$, $c_{200} = 5.27 \pm 0.46$, and with the major axis slightly inclined with respect to the line of sight of $\theta = 27.3 \pm 7.1$ deg, in agreement with the predictions of Oguri and Blandford (2009).

Sereno and Umetsu (2011) developed a method for a three-dimensional analysis of the DM halo via SL and WL data. They re-analysed the weak lensing convergence map of A1689 obtained by Umetsu and Broadhurst (2008) and Umetsu et al. (2009)

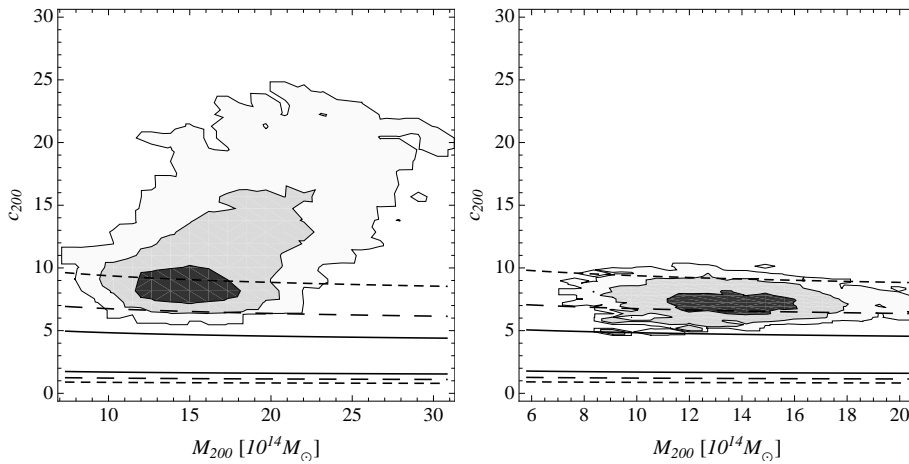


Fig. 5 Results of the combined strong and weak lensing analysis. Contour plot of the marginalised PDF for M_{200} and c_{200} for the dark matter haloes as derived under the prior assumptions of either flat axis ratio distribution and random orientation angles (left panel) or N -body like axis ratio distribution and biased orientation angles (right panel). Contours are plotted at fraction values $\exp(-2.3/2)$, $\exp(-6.17/2)$, and $\exp(-11.8/2)$ of the maximum, which denote confidence limit regions of 1, 2 and 3σ in a maximum likelihood investigation, respectively. The full, long-dashed and dashed lines enclose the 1, 2 and 3σ regions for the predicted conditional probability $c(M)$ by Duffy et al. (2008), respectively. Figure adapted from Sereno and Umetsu (2011).

on wide-field ($\sim 30' \times 24'$) Subaru data of A1689. For strong lensing, they employed a parametric lensing analysis method based on the *gravlens* kernel evaluation of χ_{SL}^2 values (Keeton 2001a, 2001b). The SL likelihood values were computed by comparing observed to predicted image positions. Several priors were considered. For the axial ratios $\eta_{\text{DM},a}$ and $\eta_{\text{DM},b}$, they considered either the N -body predictions or a flat distribution. For the alignment angle θ , they considered either the biased distribution for $p(\theta)$ (see Equ. 12) or a random distribution. For the azimuthal angle they always used a random flat distribution. For the mass, they always used a flat prior $p(M_{200}) = \text{const.}$, whereas the a priori PDF for the concentration was flat in the range $0 < c_{200} \leq 30$ and null otherwise. The theoretical $c(M)$ relation from Duffy et al. (2008) was either enforced or neglected.

Whatever the assumptions on either orientation or shape, the concentration is a bit larger but still compatible with theoretical predictions (Fig. 5). A1689 appears to be a quite typical massive cluster with a concentration in agreement with the tail at large values of the expected population of clusters of that given mass. Independently of the priors, the inferred c_{200} are only $\geq 1\sigma$ away from the predicted median value. Priors from N -body simulations also help to put an upper bound on the concentrations.

Mildly triaxial haloes do a better job in fitting data than nearly spherical lenses. Values of $0.4 \leq \eta_{\text{DM},a} \leq 0.8$ are more likely than either extremely triaxial or nearly spherical shapes. Triaxial shapes predicted by N -body simulations are in good agreement with these results. Axial ratios derived assuming a flat distribution are compatible at 1σ confidence level with predictions from N -body simulations. Furthermore, they can exclude nearly spherical shapes ($\eta_{\text{DM},a} \sim \eta_{\text{DM},b} \sim 1$) at the 3σ confidence level. Finally, they find indications for an orientation bias.

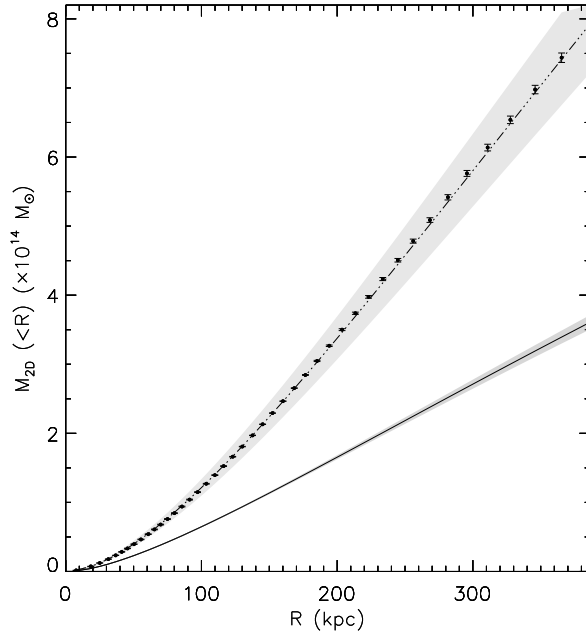


Fig. 6 2D mass enclosed within a circular aperture of radius R from lensing data (points with error bars), from an X-ray only analysis under the assumption of spherical geometry (solid line with the 1σ error grey shaded region), and from a joint X-ray+lensing analysis taking into account the 3D geometry (dot-dashed line with the 1σ error grey shaded region). In this latter case, we see that both estimates agree with each other. (Result from Morandi et al. 2011a, but updated within the full triaxial framework presented in Section 4).

The minor-major axis ratio is found in agreement with the findings by Morandi et al. (2011b), confirming a triaxial shape; yet, the value of the concentration parameter ($c_{200} = 7.3 \pm 0.8$) is a bit larger than the values presented in this review (Table 1).

Regarding the mass discrepancy, the triaxial model proposed by Morandi et al. (2011b), as well as its extension presented in this review, is able to solve the X-ray/lensing mass discrepancy. We plot in Fig. 6 the comparison between the 2D masses inferred from X-ray and lensing under spherical and triaxial models.

We have illustrated that a triaxial mass model for Abell 1689 is able to reconcile mass estimates from different probes, as well as to reproduce the large Einstein radius using Λ CDM friendly parameters. It is worth noting that the value of the inner slope of the dark matter density profile, γ , also depends on the adopted geometry. Considering Abell 1689, a standard spherical modelling leads to $\gamma = 1.16 \pm 0.04$, whereas we find $\gamma = 0.92 \pm 0.07$ using a triaxial mass model (Table 1).

5.3 The ICM Properties in a Triaxial Framework

The ICM of Abell 1689 within a triaxial model has also been the subject of interest.

De Filippis et al. (2005) and Sereno et al. (2006) investigated the ICM shape by combining X-ray and SZ observations. Given the data sets used (in particular, the absence of lensing data), error bars were pretty large and a wide range of geometries was possible: they concluded that these data sets are compatible both with a prolate and an oblate shape.

More recently, Sereno et al. (2012) implemented some significant improvements by using Bayesian inference to determine the intrinsic form: *i*) The method was still parametric but did not rely anymore on the simple isothermal β model for the X-ray data. The employed profiles can mimic complex features in either the electronic density or the temperature profile for the X-ray data. *ii*) Instead of the central Compton parameter y_0 , they considered the more reliable integrated Compton parameter. *iii*) Even if astronomical deprojection is an under-constrained problem (Sereno 2007), Sereno et al. (2012) could infer the 3D structure of the cluster using a Bayesian method without assuming any specific configuration. On the other hand in De Filippis et al. (2005) and Sereno et al. (2006), the 3D distribution was assumed to be either triaxial and aligned with the line of sight or prolate or oblate.

This method was applied to Abell 1689, where SZ and X-ray observations cover in detail a region $R \leq 1$ Mpc. The 3D electron density and temperature were modelled with parametric profiles. Distributions were assumed to be coaligned and ellipsoidal, with constant eccentricity and orientation. Intrinsic profiles were taken from Vikhlinin et al. (2006b), and Ettori et al. (2009). The metallicity was fixed to the mean observed value. The elongation e_Δ enters when 3D profiles are projected into the plane of the sky, so that fitting at once X-ray surface brightness, temperature, and the integrated Compton parameter, one can infer e_Δ as well as the parameters describing the distribution.

The combined X-ray plus SZ analysis allows to infer the width of the cluster in the plane of the sky (parametrised in terms of the ellipticity ϵ) and its size along the line of sight (expressed as the elongation e_Δ). These two observational constraints have to be used to infer the intrinsic shape of the cluster and its orientation.

Sereno et al. (2012) found a minor to major axial ratio for the ICM of 0.7 ± 0.15 , preferentially elongated along the line of sight. The hydrostatic equilibrium is not involved in their analysis since they do not derive the mass of the cluster. This value of the axis ratio is in good agreement with the one inferred by Morandi et al. (2011b) (assuming generalised hydrostatic equilibrium), who quoted a ratio for the ICM between 0.66 and 0.77 (since the method includes a radial variation of the axial ratios). This suggests that both approaches are consistent, and that the ICM in Abell 1689 is not far from being in hydrostatic equilibrium. Note that Sereno et al. (2012) use XMM data for the temperature, whereas Morandi et al. (2011b) use a Chandra temperature, which is lower than the XMM temperature by 10-20% due to calibration reasons.

It is worth noting that several processes like radiative cooling and turbulences are affecting the shape of the gas distribution more than the dark matter shape.

5.4 Overview of the Present Results on Clusters Triaxiality

So far, four clusters have been studied within the full triaxial framework described in Section 4: MACS 1423, Abell 1689, Abell 383, and Abell 1835. The results published for MACS 1423 (Morandi et al. 2010) and Abell 1689 (Morandi et al. 2011a,2011b) were derived using a triaxial model where the haloe's major axis was aligned with our line of

Table 1 Best-fit model parameters for the four clusters for which a full triaxial modelling exists. Error bars correspond to 1σ confidence level. The lines 1 – 8 refer to the best fit parameters of the DM halo: c_{200} (concentration parameter), R_s (scale radius), γ (inner DM slope), $\eta_{\text{DM},a}$ (minor-major axis ratio), $\eta_{\text{DM},b}$ (intermediate-major axis ratio), and ψ, θ, ϕ (Euler angles). The lines 9 – 14 refer to the best fit parameters $n_0, r_{c_1}, \varepsilon, \delta, r_{c_2}, v$ of the IC gas density, while the lines 15 – 16 to the best fit parameters ξ, n (normalisation and slope, respectively) of the non-thermal pressure. Finally, the last line refers to the best fit parameter \tilde{P} of the pressure at R_{200} , which is a boundary condition of the generalised HE equation (see relevant Equations in Section 4). Note that only in the case of Abell 1835 all these parameters are constrained. This is due to the inclusion of SZ data.

Cluster	Abell 1835	Abell 383	Abell 1689	MACS 1423
c_{200}	4.32 ± 0.44	4.76 ± 0.51	5.27 ± 0.46	3.97 ± 1.0
R_s (kpc)	891.0 ± 114.3	511.2 ± 73.6	683.1 ± 84.7	644.7 ± 162.1
γ	1.01 ± 0.06	1.02 ± 0.06	0.92 ± 0.07	1.06 ± 0.1
$\eta_{\text{DM},a}$	0.59 ± 0.05	0.55 ± 0.06	0.56 ± 0.07	0.62 ± 0.04
$\eta_{\text{DM},b}$	0.71 ± 0.08	0.71 ± 0.10	0.75 ± 0.08	0.72 ± 0.06
ψ (deg)	3.8 ± 4.6	-13.6 ± 5.5	-35.5 ± 13.7	-34.4 ± 5.4
θ (deg)	18.3 ± 5.2	21.1 ± 10.1	27.3 ± 7.1	34.7 ± 8.7
ϕ (deg)	-55.0 ± 6.9	-16.9 ± 15.9	-11.1 ± 6.7	-72.3 ± 8.3
n_0 (cm^{-3})	0.018 ± 0.002	0.063 ± 0.003	0.017 ± 0.001	0.15 ± 0.02
r_{c_1} (kpc)	117.7 ± 10.1	26.4 ± 1.7	119.3 ± 5.3	20.6 ± 3.1
ε	0.68 ± 0.02	0.55 ± 0.01	0.72 ± 0.02	0.55 ± 0.02
δ	0.82 ± 0.03	0.02 ± 0.01	0.33 ± 0.01	0.02 ± 0.01
r_{c_2} (kpc)	1674.3 ± 266.7	-	-	-
v	0.44 ± 0.04	-	-	-
ξ	0.177 ± 0.065	0.11 ± 0.05	0.24 ± 0.05	0.08 ± 0.03
n	0.77 ± 0.21	0	0	0
\tilde{P} (erg/cm^3)	$(2.7 \pm 0.7) \times 10^{-13}$	-	-	-

sight. Since then, the algorithm was improved and we report the results for MACS 1423 and Abell 1689 derived using the full triaxial framework. Results of the parameters for each cluster are given in Table 1. As discussed in the relevant papers, the parameters obtained through a triaxial model can be very different from the one obtained through a spherical model. In particular, regarding the concentration parameter, similar to what has been found for Abell 1689, lower values are inferred within a triaxial framework. Shown on Fig. 7 are some key properties of these four clusters: the inner slope of the dark matter density profile, and the masses and concentrations. The comparison with results from numerical simulations will be discussed in Section 6.1.

6 Discussion

6.1 (Limited) Comparison with Simulations

The parameters of a triaxial model obtained for galaxy clusters are to be compared to results from numerical simulations in order to test cosmological models. Such compar-

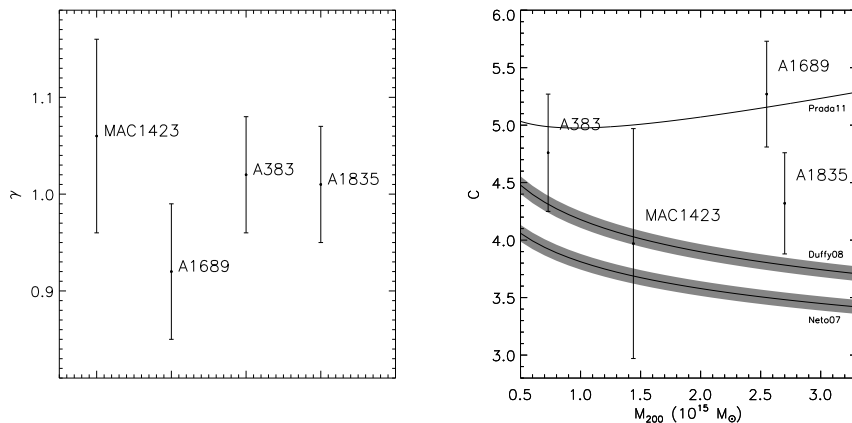


Fig. 7 Properties of the four clusters studied within the full triaxial framework described in Section 4. *Left*: inner slope of the dark matter density profile. *Right*: Masses and concentrations. Results from Λ CDM based simulations (Neto et al. 2007; Duffy et al. 2008; Prada et al. 2012) are shown. Error bars correspond to 1σ confidence levels. We caution that this comparison can be misleading since results from numerical simulations are based on a spherical assumption.

isons are routinely performed in the *spherical* case. In order to build a density profile, simulators usually do a spherical fit to their elongated profiles: they determine the enclosed mass or density assuming spherical symmetry even though the haloes are found to be triaxial and asymmetric (Section 1.1). Since triaxial analyses will have a growing importance on the observational side in the future, we advocate the need for simulations to be analysed within a triaxial framework, allowing reliable and meaningful comparisons.

Actually, the bias induced by fitting a spherical analytic formula to an elongated mass profile should be compared to the intrinsic scatter in the concentration of NFW haloes.

Having stressed the possible limitations of comparing the triaxial observational results with spherical numerical results, we can go back to Fig. 7 where some key properties of four clusters studied within a full triaxial framework are presented: the inner slope of the dark matter density profile, and the masses and concentrations. (Spherical) theoretical expectations (Neto et al. 2007; Duffy et al. 2008; Prada et al. 2012) are shown on top of the triaxial results.

Regarding inner slopes, one should keep in mind that, from the theoretical side, numerical simulations did not converge on a proper treatment of the baryonic component which is a difficult task. In this respect, when the baryonic component is taken into account, different simulations infer either a steepening or a flattening of the dark matter inner density profile (see the revue on cluster cores in this volume).

We have mentioned that simulations do not provide the relevant material to compare triaxial results to theoretical expectations. Moreover, as far as massive haloes are concerned, statistic is poor. Oguri et al. (2009) argued that the probability distribution of the concentration parameter for very massive haloes (larger than $10^{15} M_{\odot}$) and its redshift evolution had not been studied with great statistics by N-body simulations. It is worth noting that this statement also applies to extreme axis ratios in different

mass and redshift bins. Therefore, we rely on extrapolations from smaller haloes. More reliable theoretical predictions at the high mass end are needed. Recently, Prada et al. (2012) argued that previous simulation works underestimated the mean concentration at the high mass end and find an upturn in the (c,M) relation. Bhattacharya et al. (2011), in their analysis of an even larger simulation, find no evidence for such an upturn but they do find a (c,M) relation that differs in normalisation and shape from previous studies that have limited statistics in the upper mass range. Moreover, as already mentioned earlier, this upturn may be due to the inclusion of dynamically disturbed merging clusters (Ludlow et al. 2012).

The situation is changing and the most recent simulations contain a few hundreds of such haloes. For example, Angulo et al. (2012), based on the Millenium-XXL dark matter only simulation, reported 464 haloes more massive than $2 \times 10^{15} M_{\odot}$, in agreement with analytical calculations (see, *e.g.* Mortonson et al. 2011).

Another difficulty is that the expected abundance of massive haloes strongly depends on the algorithm used to find them. Angulo et al. (2012) show that this abundance changes by a factor of ~ 2 when Friends-of-Friends (Davis et al. 1985) selected subhaloes and self-bound subhaloes are compared. They argue this is in part a consequence of large haloes not forming an homogeneous population. Indeed, clusters displaying similar virial masses present a considerable diversity in shape, concentration, and amount of substructure.

To draw reliable conclusions regarding the properties of clusters and their evolution with cosmic time, we would need to study within a triaxial framework a large number of (massive) galaxy clusters. These results should be compared to predictions from simulations inferred within a triaxial framework.

6.2 On Which Scales do we Measure Triaxiality?

The scale on which a triaxial model is constrained depends on the data sets used. In the case of Abell 1835, the triaxial model has been constrained up to the virial radius thanks to the inclusion of SZ data. This question is linked with the following one: out to which radius do we have observational data with a sufficiently high signal to noise ratio? Strong lensing is limited to the very central part of a galaxy cluster. Regarding X-ray data obtained with current facilities, one can expect to reach R_{500} . Regarding weak lensing, beyond R_{500} , the signal to noise ratio becomes small, and the lensing signal estimated for a single cluster is likely to be dominated by mass not associated with this cluster, either correlated or uncorrelated (Hoekstra et al. 2011). This question is also relevant when we compare with triaxial parameters measured on simulated clusters. Ideally, we aim to compare measurements performed on the same scales.

6.3 Implementing Triaxiality in the Mass Distribution or in the Gravitational Potential?

There are two possible approaches when introducing a triaxial model for a galaxy cluster: one can either implement triaxiality directly in the mass distribution, or in the gravitational potential.

An ellipsoidal mass distribution generates isopotential surfaces which are approximated by concentric ellipsoids of decreasing axial ratio towards the outer volumes, and not of constant shape. Vice versa, if the potential is described by a triaxial ellipsoid, then the mass distribution giving birth to this potential will not be described by a triaxial ellipsoid.

Both approaches have their advantages and inconveniences and have been followed by different authors.

6.3.1 A Triaxial Mass Distribution

We have discussed in the introduction that the DM distribution behaves as an ellipsoid, being collisionless and dominating in term of mass. The dynamics of the gas (which is the second largest contribution to the mass after the DM) should be driven by the gravitational potential well of the DM. Therefore, it seems well motivated to implement triaxiality in the mass distribution as proposed in Section 4, being aware that it has its own limitations.

Recent investigations of galaxy scale dark matter haloes forming in the Aquarius simulation (Springel et al. 2008) show that the shape of a halo depends strongly on its environment, the time at which we consider it, and the radius at which we measure its shape (Vera-Ciro et al. 2011). At redshift 0, haloes exhibit a variation from prolate in the inner regions to triaxial/oblate in the outskirts, which clearly complicates the modelling. If these results are derived for galaxy scale dark matter haloes, we can expect that some of these complications also arise for cluster scale dark matter haloes. Indeed, Muñoz-Cuartas et al. (2011) found that the asphericity is more pronounced in the halo's central region (i.e. for radii smaller than 30% of the virial radius). However, internal regions are more likely to be affected by baryonic physics and therefore the inclusion of baryons is needed in order to draw more quantitative conclusions.

It is worth noting that models which involve a gravitational potential generated by an ellipsoidal mass distribution are computationally expensive.

6.3.2 A Triaxial Potential

Buote and Humphrey (2011a,2011b) investigated a different type of model where the potential, rather than the underlying mass distribution, is an ellipsoid of constant shape and orientation. They inferred analytical formulae for galaxy clusters with triaxial potential. These triaxial models themselves lead to a straightforward generalisation of analytic spherical models, and hence they are computationally fast.

In a similar fashion, Sereno et al. (2012) modelled the gas density distribution as ellipsoid of constant shape and orientation. Note that they did not make any assumption about the equilibrium of the gas.

There is both observational and theoretical work suggesting that this modelling has its limitations and which shows that the gas distribution follows isopotential surfaces approximated by concentric ellipsoids of decreasing axial ratio towards the outer volumes (Buote and Canizares 1994, 1996; Lee and Suto 2003; Hayashi et al. 2007; Morandi et al. 2010; Kawahara 2010; Deb et al. 2012).

6.3.3 So ?

It appears that, when the accuracy of the simulations or the observations increases, none of the mass distribution nor the potential can be rigorously described by a triaxial model. Indeed, Deb et al. (2012) showed in Abell 1689 that the axial ratio of both the DM and the ICM is not strictly constant with radius.

It is worth noting that, in Abell 1689, Morandi et al. and Sereno et al., using different modelling approaches find results for the shape of the ICM in pretty good agreement, which proves that both approaches are consistent and deserve additional investigation (see comparison in Section 5).

6.4 Large Einstein Radii & the Overconcentration Problem

The first claim regarding the fact that large Einstein radii may be a problem for the Λ CDM scenario was made by Broadhurst and Barkana (2008a). This claim was very constructive since it led to a number of interesting studies investigating if strong lensing clusters were over-concentrated with respect to theoretical expectations, and if the large Einstein radii observed for some extreme clusters were challenging the Λ CDM scenario. The problems of large Einstein radii and of overconcentrated clusters are somehow linked to each other: a very elongated haloe with its major axis aligned along the line of sight can lead to a highly concentrated projected surface mass density profile resulting in a large tangential critical curve, hence a large observed Einstein radius.

Oguri et al. (2009) studied the mass profiles of four clusters by combining strong and weak lensing data. The mass profiles were found to be well described by an NFW profile. They found values for the concentration parameter that are slightly higher than the Λ CDM predictions, even after taking into account the lensing bias which includes the projection effect. Taking into account the error bars they derived, the value of the concentration for each cluster is marginally consistent with theory, and the excess is not so strong compared to earlier claims. Then they add to their sample six clusters from the literature which have strong plus weak lensing analyses available. Considering the 10 clusters, they claim a 7σ excess of the concentration parameter compared with the Λ CDM predictions.

Okabe et al. (2010) conducted a weak lensing analysis of a sample of 30 X-ray luminous galaxy clusters and found a mean concentration $c_{\text{vir}} = 3.48_{-1.15}^{+1.65}$ for clusters with $M_{\text{vir}} \sim 10^{15} h^{-1} M_{\odot}$, displaying no over-concentration. However, it is worth noting that the inclusion of strong lensing data is important for an unbiased value of the concentration parameter. Indeed, background galaxy catalogues may have an uncontrolled degree of contamination from unlensed cluster members. This will dilute the shear profile in the inner region and bias low the inferred concentration parameter.

Sereno et al. (2010a) investigated the over-concentration problem on a sample of 10 strong lensing clusters. They derive which elongation along the line of sight is needed by the data in order to be compatible with the mass-concentration relation. Half of the clusters of their sample support the expectation from Λ CDM simulations, being triaxial haloes with a strong orientation bias. The other half would fit the mass-concentration relation only if they were characterised by a filamentary structure extremely elongated along the line of sight, which the authors consider very unlikely considering standard scenarios of structure formations.

Oguri et al. (2012) studied the mass distribution of 28 galaxy clusters using strong and weak lensing observations. The sample is made of clusters selected via their strong lensing properties: the Sloan Giant Arc Survey. They found the inferred mass-concentration relation for these clusters to be in reasonable agreement with the simulations for very massive haloes ($M_{\text{vir}} \sim 10^{15} h^{-1} M_{\odot}$). However, they found that the observed concentrations are much higher than theoretical expectations for less massive haloes ($M_{\text{vir}} \sim 10^{14} h^{-1} M_{\odot}$), even after taking into account the mass dependence of the lensing bias.

We have seen that, even after accounting for projection biases, an over-concentration problem remains in some lensing clusters (see also Gralla et al. 2011).

Another problem concerns the *number* of over-concentrated clusters one can find in a given survey. This is an open question worth investigating in detail. We have seen that Abell 1689 by itself does not pose a severe challenge to the Λ CDM model, but such high values of the concentration parameter appear to be common in the combined strong plus weak lensing analyses of massive clusters.

We now come back to the Einstein radius, which provides a relatively model-independent measure of the mass density of a cluster core, and is observationally easier to infer than the concentration parameter. To date, the largest Einstein radius has been observed in MACS J0717.5+3745, hereafter MACS J0717 (Zitrin et al. 2009; Limousin et al. 2012). Its effective Einstein radius was estimated to be $55 \pm 3''$ for a source redshift of $z \sim 2.5$. Zitrin et al. (2009) claimed that the probability to find such a system in a Λ CDM Universe is very unlikely, of the order of 10^{-7} . Recently, Waizmann et al. (2012) modeled the distribution function of the single largest measured value of the Einstein radius in a given cosmological volume based on a Monte Carlo approach. Results are fitted with the general extreme value distribution. They showed that the large Einstein radius in MACS J0717 does not exhibit tension with Λ CDM, even if they neglect the impact of dynamical merging which is clearly established for MACS J0717, and which would allow large Einstein radii more likely to be found (Redlich et al. 2012). This finding is at odds with the claims by Zitrin et al. (2009), and we refer the reader to Waizmann et al. (2012) for a discussion of the difference of calculations between each studies. They concluded that, for an observed Einstein radius to challenge Λ CDM, one should observe Einstein radii larger than $100''$.

Besides, Waizmann et al. (2012) investigated the influence of triaxiality on the resulting extreme value distributions of the largest Einstein radii, and find that it is very sensitive to very elongated objects. In agreement with Oguri and Blandford (2009), they confirm that the single largest Einstein radius has not necessarily its origin in the most massive clusters. Instead, triaxiality, together with the halo orientation, has a stronger impact than the mass of the cluster itself.

6.5 Triaxiality & Self Interacting DM

The asphericity of galaxy cluster scale DM haloes demonstrates that the self-interaction of DM particles cannot be too large. Yoshida et al. (2000) investigated how the internal structure of dark haloes is affected if cold dark matter particles are assumed to have a large cross section for elastic collisions. It results in a cluster that is more nearly spherical at all radii compared to the collisionless case. More recently, Peter et al. (2012) and Rocha et al. (2012) presented cosmological simulations with self-interacting

dark matter (SIDM). They showed that the currently observed asphericity allow dark matter self-interaction cross section at least as large as $\sigma/m = 0.1 \text{ cm}^2/\text{g}$.

6.6 Dynamical Information

A spectroscopic campaign targeting cluster members is highly relevant when studying a galaxy cluster and its 3D geometry. Indeed, it can give us some clues about the dynamical state of the system. This is particularly relevant since the more relaxed and unimodal the cluster, the more legitimate to describe it with a single mass clump (whatever the geometry considered).

For example, in the galaxy cluster Cl0024, an apparently relaxed cluster in X-ray and lensing data sets, Czoske et al. (2001) discovered that this cluster is composed of two mass clumps aligned along the line of sight and argued that a high-speed collision had taken place (Czoske et al. 2002).

7 Conclusions: Galaxy Clusters are *not* Triaxial

We have discussed that a triaxial model is clearly an important step forward to describe galaxy clusters more realistically than using a spherical model.

However, as any model, it has its own limitations we aim to mention. We have seen in Section 6.3 that, when looking at details, haloes exhibit departures from a simple triaxial geometry. Both observations and simulations show the presence of substructures which are not accounted for by a triaxial model for the galaxy cluster. If the substructures are small compared to the main cluster's halo, then the triaxial approximation may be accurate enough. On the other hand, unrelaxed haloes often have shapes that are not adequately described by ellipsoids, making shape parameters ill-defined. Indeed, if there is no clear dominant halo but a superposition of sub-haloes with comparable masses, the triaxial approximation may be questionable. For example, the high redshift MACS clusters (Ebeling et al. 2007) which are found to be highly disturbed (Ebeling et al. 2004; Kartaltepe et al. 2008; Smith et al. 2009; Zitrin and Broadhurst 2009; Zitrin et al. 2009, 2010; Mann and Ebeling 2011; Limousin et al. 2012) are unlikely to be well described by a triaxial halo, as proposed by Sereno and Zitrin (2012). We note, however, that the latter study constitutes a step forward with respect to a spherical analysis. Therefore, we emphasise the fact that, in order to apply a triaxial mass model, one should concentrate on unimodal galaxy clusters with little substructures and as close as possible to virialization.

We have presented in this review results obtained in a triaxial framework for four strong lensing clusters. To draw serious conclusions regarding the clusters' properties and how they might evolve with time, or with any characteristic of the cluster, we need to study within a triaxial framework a sample of clusters as large as possible. Current cluster samples, which already have complementary data sets, can allow such an ambitious project to be started: the Local Cluster Substructure Survey (LoCuSS Smith et al. 2010)¹; the MAAssive Cluster Survey (MACS Ebeling et al. 2001); the Clus-

¹ <http://www.sr.bham.ac.uk/locuss/>

ter Lensing And Supernova survey with Hubble (CLASH Postman et al. 2012)²; and the Dark energy American French Team sample (DAFT Guennou et al. 2010, 2012)³.

As mentioned earlier, a triaxial model is still a simplification of what a galaxy cluster might be. It is not clear how departures from a strict triaxial geometry can bias results based on the assumption of a triaxial model. Actually, this ought to be tested using numerically simulated clusters: mock lensing, X-ray and SZ observations can be generated (*e.g.* Rasia et al. 2012) for galaxy clusters presenting different dynamical states, and analysed in the same way as observational data. Comparing the inferred triaxial parameters to those measured on the simulated haloes is essential to test the methods and to quantify how the presence of substructures and deviations from equilibrium can bias triaxial reconstructions. This pioneering work will also pave the road to more refined mass models beyond the triaxial framework.

Acknowledgements ML acknowledges the Centre National de la Recherche Scientifique (CNRS) for its support. The Dark Cosmology Centre is funded by the Danish National Research Foundation. T.V. acknowledges support from CONACYT grant 165365 through the program Estancias posdoctorales y sabáticas al extranjero para la consolidación de grupos de investigación. We thank the International Space Science Institute at Berne, Switzerland (ISSI) for providing to our group very good working conditions.

References

- S.M.K. Alam, B.S. Ryden, The Shapes of Galaxies in the Sloan Digital Sky Survey. *ApJ* **570**, 610–617 (2002). doi:10.1086/339790
- B. Allgood, R.A. Flores, J.R. Primack, A.V. Kravtsov, R.H. Wechsler, A. Faltenbacher, J.S. Bullock, The shape of dark matter haloes: dependence on mass, redshift, radius and formation. *367*, 1781–1796 (2006). doi:10.1111/j.1365-2966.2006.10094.x
- J.R. Allison, A.C. Taylor, M.E. Jones, S. Rawlings, S.T. Kay, A parametric physical model for the intracluster medium and its use in joint SZ/X-ray analyses of galaxy clusters. *410*, 341–358 (2011). doi:10.1111/j.1365-2966.2010.17447.x
- G. Altay, J.M. Colberg, R.A.C. Croft, The influence of large-scale structures on halo shapes and alignments. *370*, 1422–1428 (2006). doi:10.1111/j.1365-2966.2006.10555.x
- S. Ameglio, S. Borgani, E. Pierpaoli, K. Dolag, Joint deprojection of Sunyaev-Zeldovich and X-ray images of galaxy clusters. *382*, 397–411 (2007). doi:10.1111/j.1365-2966.2007.12384.x
- S. Ameglio, S. Borgani, E. Pierpaoli, K. Dolag, S. Ettori, A. Morandi, Reconstructing mass profiles of simulated galaxy clusters by combining Sunyaev-Zeldovich and X-ray images. *394*, 479–490 (2009). doi:10.1111/j.1365-2966.2008.14324.x
- K.E. Andersson, G.M. Madejski, Complex Structure of Galaxy Cluster A1689: Evidence for a Merger from X-Ray Data? *Astrophys. J.* **607**, 190–201 (2004). doi:10.1086/383258
- R.E. Angulo, V. Springel, S.D.M. White, A. Jenkins, C.M. Baugh, C.S. Frenk, Scaling relations for galaxy clusters in the Millennium-XXL simulation. *ArXiv e-prints* (2012)
- M.A. Aragón-Calvo, R. van de Weygaert, B.J.T. Jones, J.M. van der Hulst, Spin Alignment of Dark Matter Halos in Filaments and Walls. *655*, 5–8 (2007). doi:10.1086/511633
- J. Bailin, M. Steinmetz, Internal and External Alignment of the Shapes and Angular Momenta of Λ CDM Halos. *Astrophys. J.* **627**, 647–665 (2005). doi:10.1086/430397
- S. Bardeau, J.-P. Kneib, O. Czoske, G. Soucail, I. Smail, H. Ebeling, G.P. Smith, A CFH12k lensing survey of X-ray luminous galaxy clusters. I. Weak lensing methodology. *Astron. Astrophys.* **434**, 433–448 (2005). doi:10.1051/0004-6361:20041643
- S. Basilakos, M. Plionis, S.J. Maddox, The apparent and intrinsic shape of the APM galaxy clusters. *MNRAS* **316**, 779–785 (2000)
- K. Basu, Y.-Y. Zhang, M.W. Sommer, A.N. Bender, F. Bertoldi, M. Dobbs, H. Eckmiller, N.W. Halverson, W.L. Holzappel, C. Horellou, V. Jaritz, D. Johansson, B. Johnson, J.

² <http://www.stsci.edu/postman/CLASH/Home.html>

³ <http://cencos.oamp.fr/DAFT/>

- Kennedy, R. Kneissl, T. Lanting, A.T. Lee, J. Mehl, K.M. Menten, F.P. Navarrete, F. Pacaud, C.L. Reichardt, T.H. Reiprich, P.L. Richards, D. Schwan, B. Westbrook, Non-parametric modeling of the intra-cluster gas using APEX-SZ bolometer imaging data. *Astron. Astrophys.* **519**, 29 (2010). doi:10.1051/0004-6361/200913334
- P. Bett, V. Eke, C.S. Frenk, A. Jenkins, J. Helly, J. Navarro, The spin and shape of dark matter haloes in the Millennium simulation of a Λ cold dark matter universe. **376**, 215–232 (2007). doi:10.1111/j.1365-2966.2007.11432.x
- S. Bhattacharya, S. Habib, K. Heitmann, Dark Matter Halo Profiles of Massive Clusters: Theory vs. Observations. ArXiv e-prints (2011)
- B. Binggeli, On the intrinsic shape of elliptical galaxies. *A&A* **82**, 289–294 (1980)
- B. Binggeli, The shape and orientation of clusters of galaxies. *Astron. Astrophys.* **107**, 338–349 (1982)
- J. Binney, G. de Vaucouleurs, The apparent and true ellipticities of galaxies of different Hubble types in the Second Reference Catalogue. *MNRAS* **194**, 679–691 (1981)
- J. Binney, S. Tremaine, *Galactic Dynamics* (Princeton, NJ, Princeton University Press, 1987, 747 p., ???, 1987)
- M. Bradač, T. Schrabback, T. Erben, M. McCourt, E. Million, A. Mantz, S. Allen, R. Blandford, A. Halkola, H. Hildebrandt, M. Lombardi, P. Marshall, P. Schneider, T. Treu, J.-P. Kneib, Dark Matter and Baryons in the X-Ray Luminous Merging Galaxy Cluster RX J1347.5-1145. *Astrophys. J.* **681**, 187–196 (2008). doi:10.1086/588377
- T.J. Broadhurst, R. Barkana, Large Einstein radii: a problem for Λ CDM. **390**, 1647–1654 (2008a). doi:10.1111/j.1365-2966.2008.13852.x
- T.J. Broadhurst, R. Barkana, Large Einstein radii: a problem for Λ CDM. **390**, 1647–1654 (2008b). doi:10.1111/j.1365-2966.2008.13852.x
- R. Brunino, I. Trujillo, F.R. Pearce, P.A. Thomas, The orientation of galaxy dark matter haloes around cosmic voids. **375**, 184–190 (2007). doi:10.1111/j.1365-2966.2006.11282.x
- J.S. Bullock, T.S. Kolatt, Y. Sigad, R.S. Somerville, A.V. Kravtsov, A.A. Klypin, J.R. Primack, A. Dekel, Profiles of dark haloes: evolution, scatter and environment. **321**, 559–575 (2001). doi:10.1046/j.1365-8711.2001.04068.x
- D.A. Buote, C.R. Canizares, X-ray constraints on the shape of the dark matter in five Abell clusters. *Astrophys. J.* **400**, 385–397 (1992). doi:10.1086/172004
- D.A. Buote, C.R. Canizares, Geometrical evidence for dark matter: X-ray constraints on the mass of the elliptical galaxy NGC 720. *Astrophys. J.* **427**, 86–111 (1994). doi:10.1086/174123
- D.A. Buote, C.R. Canizares, X-Ray Constraints on the Intrinsic Shapes and Baryon Fractions of Five Abell Clusters. *Astrophys. J.* **457**, 565 (1996). doi:10.1086/176753
- D.A. Buote, P.J. Humphrey, Spherically averaging ellipsoidal galaxy clusters in X-ray and Sunyaev-Zel’dovich studies - I. Analytical relations. 2136(2011a). doi:10.1111/j.1365-2966.2011.20163.x
- D.A. Buote, P.J. Humphrey, Spherically Averaging Ellipsoidal Galaxy Clusters in X-Ray and Sunyaev-Zel’dovich Studies: II. Biases. ArXiv e-prints(2011b)
- M. Cappellari, E. Emsellem, R. Bacon, M. Bureau, R.L. Davies, P.T. de Zeeuw, J. Falcón-Barroso, D. Krajnović, H. Kuntschner, R.M. McDermid, R.F. Peletier, M. Sarzi, R.C.E. van den Bosch, G. van de Ven, The SAURON project - X. The orbital anisotropy of elliptical and lenticular galaxies: revisiting the $(V/\sigma, \epsilon)$ diagram with integral-field stellar kinematics. **379**, 418–444 (2007). doi:10.1111/j.1365-2966.2007.11963.x
- D. Carter, N. Metcalfe, The morphology of clusters of galaxies. **191**, 325–337 (1980)
- D. Chakrabarty, E. de Filippis, H. Russell, Cluster geometry and inclinations from deprojection uncertainties. Cluster geometry and inclination. *Astron. Astrophys.* **487**, 75–87 (2008). doi:10.1051/0004-6361:200809510
- D. Clowe, Wide-Field Weak Lensing Cluster Mass Reconstructions, in *Astronomical Society of the Pacific Conference Series*, ed. by S. Bowyer, C.-Y. Hwang, 2003, p. 271
- D. Clowe, G. De Lucia, L. King, Effects of asphericity and substructure on the determination of cluster mass with weak gravitational lensing. **350**, 1038–1048 (2004). doi:10.1111/j.1365-2966.2004.07723.x
- S. Cole, C. Lacey, The structure of dark matter haloes in hierarchical clustering models. **281**, 716 (1996)
- A.R. Cooray, Galaxy clusters: oblate or prolate? *MNRAS* **313**, 783–788 (2000)
- V.L. Corless, L.J. King, A statistical study of weak lensing by triaxial dark matter

- haloes: consequences for parameter estimation. **380**, 149–161 (2007). doi:10.1111/j.1365-2966.2007.12018.x
- V.L. Corless, L.J. King, An MCMC fitting method for triaxial dark matter haloes. **390**, 997–1013 (2008). doi:10.1111/j.1365-2966.2008.13744.x
- V.L. Corless, L.J. King, D. Clowe, A new look at massive clusters: weak lensing constraints on the triaxial dark matter haloes of A1689, A1835 and A2204. **393**, 1235–1254 (2009). doi:10.1111/j.1365-2966.2008.14294.x
- O. Czoske, Wide-field Spectroscopy of A1689 and A1835 with Vimos: First Results, in *IAU Colloq. 195: Outskirts of Galaxy Clusters: Intense Life in the Suburbs*, ed. by A. Diaferio, 2004, pp. 183–187. doi:10.1017/S1743921304000390
- O. Czoske, J.-P. Kneib, G. Soucail, T.J. Bridges, Y. Mellier, J.-C. Cuillandre, A wide-field spectroscopic survey of the cluster of galaxies $\text{jASTROBJ}_{\text{C}}\text{C10024+1654}/\text{ASTROBJ}_{\text{C}}$. I. The catalogue. *Astron. Astrophys.* **372**, 391–405 (2001). doi:10.1051/0004-6361:20010398
- O. Czoske, B. Moore, J.-P. Kneib, G. Soucail, A wide-field spectroscopic survey of the cluster of galaxies $\text{jASTROBJ}_{\text{C}}\text{C10024+1654}/\text{ASTROBJ}_{\text{C}}$. II. A high-speed collision? *Astron. Astrophys.* **386**, 31–41 (2002). doi:10.1051/0004-6361:20020230
- M. Davis, G. Efstathiou, C.S. Frenk, S.D.M. White, The evolution of large-scale structure in a universe dominated by cold dark matter. *Astrophys. J.* **292**, 371–394 (1985). doi:10.1086/163168
- E. De Filippis, M. Sereno, M.W. Bautz, G. Longo, Measuring the Three-dimensional Structure of Galaxy Clusters. I. Application to a Sample of 25 Clusters. *Astrophys. J.* **625**, 108–120 (2005). doi:10.1086/429401
- P.A.M. de Theije, P. Katgert, E. van Kampen, The shapes of galaxy clusters. *MNRAS* **273**, 30–46 (1995)
- S. Deb, A. Morandi, K. Pedersen, S. Riemer-Sorensen, D.M. Goldberg, H. Dahle, Mass Reconstruction using Particle Based Lensing II: Quantifying substructure with Strong+Weak lensing and X-rays. ArXiv e-prints (2012)
- A. Donnarumma, S. Ettori, M. Meneghetti, R. Gavazzi, B. Fort, L. Moscardini, A. Romano, L. Fu, F. Giordano, M. Radovich, R. Maoli, R. Scaramella, J. Richard, Abell 611. II. X-ray and strong lensing analyses. *Astron. Astrophys.* **528**, 73 (2011). doi:10.1051/0004-6361/201014120
- A.G. Doroshkevich, Spatial structure of perturbations and origin of galactic rotation in fluctuation theory. *Astrophysics* **6**, 320–330 (1970). doi:10.1007/BF01001625
- J. Dubinski, The Origin of the Brightest Cluster Galaxies. *Astrophys. J.* **502**, 141 (1998). doi:10.1086/305901
- J. Dubinski, R.G. Carlberg, The structure of cold dark matter halos. *Astrophys. J.* **378**, 496–503 (1991). doi:10.1086/170451
- A.R. Duffy, J. Schaye, S.T. Kay, C. Dalla Vecchia, Dark matter halo concentrations in the Wilkinson Microwave Anisotropy Probe year 5 cosmology. **390**, 64–68 (2008). doi:10.1111/j.1745-3933.2008.00537.x
- H. Ebeling, E. Barrett, D. Donovan, Discovery of a Large-Scale Filament Connected to the Massive Galaxy Cluster MACS J0717.5+3745 at $z=0.551$. **609**, 49–52 (2004). doi:10.1086/422750
- H. Ebeling, A.C. Edge, J.P. Henry, MACS: A Quest for the Most Massive Galaxy Clusters in the Universe. *Astrophys. J.* **553**, 668–676 (2001). doi:10.1086/320958
- H. Ebeling, E. Barrett, D. Donovan, C.-J. Ma, A.C. Edge, L. van Speybroeck, A Complete Sample of 12 Very X-Ray Luminous Galaxy Clusters at z 0.5. **661**, 33–36 (2007). doi:10.1086/518603
- H. Ebeling, A.C. Edge, A. Mantz, E. Barrett, J.P. Henry, C.J. Ma, L. van Speybroeck, The X-ray brightest clusters of galaxies from the Massive Cluster Survey. **407**, 83–93 (2010). doi:10.1111/j.1365-2966.2010.16920.x
- V.R. Eke, J.F. Navarro, M. Steinmetz, The Power Spectrum Dependence of Dark Matter Halo Concentrations. *Astrophys. J.* **554**, 114–125 (2001). doi:10.1086/321345
- S. Ettori, A. Morandi, P. Tozzi, I. Balestra, S. Borgani, P. Rosati, L. Lovisari, F. Terenziani, The cluster gas mass fraction as a cosmological probe: a revised study. *Astron. Astrophys.* **501**, 61–73 (2009). doi:10.1051/0004-6361/200810878
- A.K.D. Evans, S. Bridle, A Detection of Dark Matter Halo Ellipticity using Galaxy Cluster Lensing in the SDSS. *Astrophys. J.* **695**, 1446–1456 (2009). doi:10.1088/0004-637X/695/2/1446
- A.E. Evrard, T.J. MacFarland, H.M.P. Couchman, J.M. Colberg, N. Yoshida, S.D.M. White, A.

- Jenkins, C.S. Frenk, F.R. Pearce, J.A. Peacock, P.A. Thomas, Galaxy Clusters in Hubble Volume Simulations: Cosmological Constraints from Sky Survey Populations. *Astrophys. J.* **573**, 7–36 (2002). doi:10.1086/340551
- D. Fabricant, G. Rybicki, P. Gorenstein, X-ray measurements of the nonspherical mass distribution in the cluster of galaxies A2256. *Astrophys. J.* **286**, 186–195 (1984). doi:10.1086/162586
- G. Fasano, R. Vio, Apparent and true flattening distribution of elliptical galaxies. *MNRAS* **249**, 629–633 (1991)
- D.C. Fox, U.-L. Pen, The Distance to Clusters: Correcting for Asphericity. *Astrophys. J.* **574**, 38–50 (2002). doi:10.1086/340897
- C.S. Frenk, S.D.M. White, M. Davis, G. Efstathiou, The formation of dark halos in a universe dominated by cold dark matter. *Astrophys. J.* **327**, 507–525 (1988). doi:10.1086/166213
- L. Gao, J.F. Navarro, S. Cole, C.S. Frenk, S.D.M. White, V. Springel, A. Jenkins, A.F. Neto, The redshift dependence of the structure of massive Λ cold dark matter haloes. **387**, 536–544 (2008). doi:10.1111/j.1365-2966.2008.13277.x
- L. Gao, J.F. Navarro, C.S. Frenk, A. Jenkins, V. Springel, S.D.M. White, The Phoenix Project: the Dark Side of Rich Galaxy Clusters. *ArXiv e-prints* (2012)
- R. Gavazzi, Projection effects in cluster mass estimates: the case of MS2137-23. *Astron. Astrophys.* **443**, 793–804 (2005). doi:10.1051/0004-6361:20053166
- N. Gehrels, Confidence limits for small numbers of events in astrophysical data. *Astrophys. J.* **303**, 336–346 (1986). doi:10.1086/164079
- M. Gitti, F. Brighenti, B.R. McNamara, Evidence for AGN Feedback in Galaxy Clusters and Groups. *Advances in Astronomy* **2012** (2012). doi:10.1155/2012/950641
- M.B. Gralla, K. Sharon, M.D. Gladders, D.P. Marrone, L.F. Barrientos, M. Bayliss, M. Bonamente, E. Bulbul, J.E. Carlstrom, T. Culverhouse, D.G. Gilbank, C. Greer, N. Hasler, D. Hawkins, R. Hennessy, M. Joy, B. Koester, J. Lamb, E. Leitch, A. Miller, T. Mroczkowski, S. Muchojev, M. Oguri, T. Plagge, C. Pryke, D. Woody, Sunyaev-Zel'dovich Effect Observations of Strong Lensing Galaxy Clusters: Probing the Overconcentration Problem. *Astrophys. J.* **737**, 74 (2011). doi:10.1088/0004-637X/737/2/74
- L. Guennou, C. Adami, M.P. Ulmer, V. Lebrun, F. Durret, D. Johnston, O. Ilbert, D. Clowe, R. Gavazzi, K. Murphy, T. Schrabback, S. Allam, J. Annis, S. Basa, C. Benoist, A. Biviano, A. Cappi, J.M. Kubo, P. Marshall, A. Mazure, F. Rostagni, D. Russeil, E. Slezak, The DAFT/FADA survey. I. Photometric redshifts along lines of sight to clusters in the $z = [0.4, 0.9]$ interval. *Astron. Astrophys.* **523**, 21 (2010). doi:10.1051/0004-6361/201015174
- L. Guennou, C. Adami, C. Da Rocha, F. Durret, M.P. Ulmer, S. Allam, S. Basa, C. Benoist, A. Biviano, D. Clowe, R. Gavazzi, C. Halliday, O. Ilbert, D. Johnston, D. Just, R. Kron, J.M. Kubo, V. Le Brun, P. Marshall, A. Mazure, K.J. Murphy, D.N.E. Pereira, C.R. Rabaça, F. Rostagni, G. Rudnick, D. Russeil, T. Schrabback, E. Slezak, D. Tucker, D. Zaritsky, Intracluster light in clusters of galaxies at redshifts 0.4 z 0.8. *Astron. Astrophys.* **537**, 64 (2012). doi:10.1051/0004-6361/201117482
- A. Halkola, S. Seitz, M. Pannella, Parametric strong gravitational lensing analysis of Abell 1689. **372**, 1425–1462 (2006). doi:10.1111/j.1365-2966.2006.10948.x
- E. Hayashi, J.F. Navarro, V. Springel, The shape of the gravitational potential in cold dark matter haloes. **377**, 50–62 (2007). doi:10.1111/j.1365-2966.2007.11599.x
- J.F. Hennawi, N. Dalal, P. Bode, J.P. Ostriker, Characterizing the Cluster Lens Population. *Astrophys. J.* **654**, 714–730 (2007). doi:10.1086/497362
- H. Hoekstra, J. Hartlap, S. Hilbert, E. van Uitert, Effects of distant large-scale structure on the precision of weak lensing mass measurements. **412**, 2095–2103 (2011). doi:10.1111/j.1365-2966.2010.18053.x
- P.F. Hopkins, N.A. Bahcall, P. Bode, Cluster Alignments and Ellipticities in Λ CDM Cosmology. *Astrophys. J.* **618**, 1–15 (2005). doi:10.1086/425993
- E.P. Hubble, Extragalactic nebulae. *ApJ* **64**, 321–369 (1926)
- N. Itoh, Y. Kohyama, S. Nozawa, Relativistic Corrections to the Sunyaev-Zeldovich Effect for Clusters of Galaxies. *Astrophys. J.* **502**, 7 (1998). doi:10.1086/305876
- Y.P. Jing, Y. Suto, Triaxial Modeling of Halo Density Profiles with High-Resolution N-Body Simulations. *Astrophys. J.* **574**, 538–553 (2002). doi:10.1086/341065
- E. Jullo, J.-P. Kneib, M. Limousin, Á. Elíasdóttir, P.J. Marshall, T. Verdugo, A Bayesian approach to strong lensing modelling of galaxy clusters. *New Journal of Physics* **9**, 447 (2007). doi:10.1088/1367-2630/9/12/447
- J.S. Kartaltepe, H. Ebeling, C.J. Ma, D. Donovan, Probing the large-scale structure around

- the most distant galaxy clusters from the massive cluster survey. **389**, 1240–1248 (2008). doi:10.1111/j.1365-2966.2008.13620.x
- S.F. Kasun, A.E. Evrard, Shapes and Alignments of Galaxy Cluster Halos. *Astrophys. J.* **629**, 781–790 (2005). doi:10.1086/430811
- H. Kawahara, The Axis Ratio Distribution of X-ray Clusters Observed by XMM-Newton. *Astrophys. J.* **719**, 1926–1931 (2010). doi:10.1088/0004-637X/719/2/1926
- M. Kawaharada, N. Okabe, K. Umetsu, M. Takizawa, K. Matsushita, Y. Fukazawa, T. Hamana, S. Miyazaki, K. Nakazawa, T. Ohashi, Suzaku Observation of A1689: Anisotropic Temperature and Entropy Distributions Associated with the Large-scale Structure. *Astrophys. J.* **714**, 423–441 (2010). doi:10.1088/0004-637X/714/1/423
- C.R. Keeton, A Catalog of Mass Models for Gravitational Lensing. astro-ph/0102341(2001a)
- C.R. Keeton, Computational Methods for Gravitational Lensing. astro-ph/0102340(2001b)
- L.J. King, D.I. Clowe, P. Schneider, Parameterised models for the lensing cluster Abell 1689. *Astron. Astrophys.* **383**, 118–124 (2002). doi:10.1051/0004-6361:20011722
- T. Kitayama, E. Komatsu, N. Ota, T. Kuwabara, Y. Suto, K. Yoshikawa, M. Hattori, H. Matsuo, Exploring Cluster Physics with High-Resolution Sunyaev–Zel’dovich Effect Images and X-Ray Data: The Case of the Most X-Ray-Luminous Galaxy Cluster RX J1347-1145. **56**, 17–28 (2004)
- E.T. Lau, A.V. Kravtsov, D. Nagai, Residual Gas Motions in the Intracluster Medium and Bias in Hydrostatic Measurements of Mass Profiles of Clusters. *Astrophys. J.* **705**, 1129–1138 (2009). doi:10.1088/0004-637X/705/2/1129
- E.T. Lau, D. Nagai, A.V. Kravtsov, A. Vikhlinin, A.R. Zentner, Constraining Cluster Physics with the Shape of X-ray Clusters: Comparison of Local X-ray Clusters versus LCDM Clusters. ArXiv e-prints (2012)
- J. Lee, Y. Suto, Modeling Intracluster Gas in Triaxial Dark Halos: An Analytic Approach. *Astrophys. J.* **585**, 151–160 (2003). doi:10.1086/345931
- J. Lee, Y. Suto, Reconstructing the Three-dimensional Structure of Underlying Triaxial Dark Halos from X-Ray and Sunyaev-Zel’dovich Effect Observations of Galaxy Clusters. *Astrophys. J.* **601**, 599–609 (2004). doi:10.1086/380506
- J. Lee, Y.P. Jing, Y. Suto, An Analytic Model for the Axis Ratio Distribution of Dark Matter Halos from the Primordial Gaussian Density Field. *Astrophys. J.* **632**, 706–712 (2005). doi:10.1086/444345
- D. Lenze, R. Barkana, T.J. Broadhurst, Y. Rephaeli, Mass and gas profiles in A1689: joint X-ray and lensing analysis. **386**, 1092–1106 (2008). doi:10.1111/j.1365-2966.2008.13116.x
- M. Limousin, J. Richard, E. Jullo, J.-P. Kneib, B. Fort, G. Soucail, A. Elíasdóttir, P. Nataraajan, R.S. Ellis, I. Smail, O. Czoske, G.P. Smith, P. Hudelot, S. Bardeau, H. Ebeling, E. Egami, K.K. Knudsen, Combining Strong and Weak Gravitational Lensing in Abell 1689. *Astrophys. J.* **668**, 643–666 (2007). doi:10.1186/383259
- M. Limousin, J. Richard, J.-P. Kneib, H. Brink, R. Pelló, E. Jullo, H. Tu, J. Sommer-Larsen, E. Egami, M.J. Michałowski, R. Cabanac, D.P. Stark, Strong lensing in Abell 1703: constraints on the slope of the inner distribution. *Astron. Astrophys.* **489**, 23–35 (2008). doi:10.1051/0004-6361:200809646
- M. Limousin, H. Ebeling, J. Richard, A.M. Swinbank, G.P. Smith, M. Jauzac, S. Rodionov, C.-J. Ma, I. Smail, A.C. Edge, E. Jullo, J.-P. Kneib, Strong lensing by a node of the cosmic web. The core of MACS J0717.5+3745 at $z = 0.55$. *Astron. Astrophys.* **544**, 71 (2012). doi:10.1051/0004-6361/201117921
- E.L. Lokas, F. Prada, R. Wojtak, M. Moles, S. Gottlöber, The complex velocity distribution of galaxies in Abell 1689: implications for mass modelling. **366**, 26–30 (2006). doi:10.1111/j.1745-3933.2005.00125.x
- A.D. Ludlow, J.F. Navarro, M. Li, R.E. Angulo, M. Boylan-Kolchin, P.E. Bett, The Dynamical State and Mass-Concentration Relation of Galaxy Clusters. ArXiv e-prints (2012)
- A.V. Macciò, A.A. Dutton, F.C. van den Bosch, Concentration, spin and shape of dark matter haloes as a function of the cosmological model: WMAP1, WMAP3 and WMAP5 results. **391**, 1940–1954 (2008). doi:10.1111/j.1365-2966.2008.14029.x
- A. Mahdavi, W. Chang, Model-independent Limits on the Line-of-sight Depth of Clusters of Galaxies Using X-Ray and Sunyaev-Zel’dovich data. **735**, 4 (2011). doi:10.1088/2041-8205/735/1/L4
- A. Mahdavi, H. Hoekstra, A. Babul, J. Sievers, S.T. Myers, J.P. Henry, Joint Analysis of Clus-

- ter Observations. I. Mass Profile of Abell 478 from Combined X-Ray, Sunyaev-Zel'dovich, and Weak-Lensing Data. *Astrophys. J.* **664**, 162–180 (2007). doi:10.1086/517958
- A. Mahdavi, H. Hoekstra, A. Babul, J.P. Henry, Evidence for non-hydrostatic gas from the cluster X-ray to lensing mass ratio. **384**, 1567–1574 (2008). doi:10.1111/j.1365-2966.2007.12796.x
- A.W. Mann, H. Ebeling, X-ray/optical classification of cluster mergers and the evolution of the cluster merger fraction. *ArXiv e-prints* (2011)
- P.J. Marshall, M.P. Hobson, A. Slosar, Bayesian joint analysis of cluster weak lensing and Sunyaev-Zel'dovich effect data. **346**, 489–500 (2003). doi:10.1046/j.1365-2966.2003.07111.x
- P. Mazzotta, E. Rasia, L. Moscardini, G. Tormen, Comparing the temperatures of galaxy clusters from hydrodynamical N-body simulations to Chandra and XMM-Newton observations. **354**, 10–24 (2004). doi:10.1111/j.1365-2966.2004.08167.x
- E. Medezinski, T. Broadhurst, K. Umetsu, D. Coe, N. Benítez, H. Ford, Y. Rephaeli, N. Arimoto, X. Kong, Using Weak-Lensing Dilution to Improve Measurements of the Luminous and Dark Matter in A1689. *Astrophys. J.* **663**, 717–733 (2007). doi:10.1086/518638
- M. Meneghetti, M. Bartelmann, L. Moscardini, cD galaxy contribution to the strong lensing cross-sections of galaxy clusters. **346**, 67–77 (2003). doi:10.1046/j.1365-2966.2003.07068.x
- M. Meneghetti, N. Yoshida, M. Bartelmann, L. Moscardini, V. Springel, G. Tormen, S.D.M. White, Giant cluster arcs as a constraint on the scattering cross-section of dark matter. **325**, 435–442 (2001). doi:10.1046/j.1365-8711.2001.04477.x
- M. Meneghetti, C. Fedeli, F. Pace, S. Gottlöber, G. Yepes, Strong lensing in the MARENOSTRUM UNIVERSE. I. Biases in the cluster lens population. *Astron. Astrophys.* **519**, 90 (2010a). doi:10.1051/0004-6361/201014098
- M. Meneghetti, E. Rasia, J. Merten, F. Bellagamba, S. Ettori, P. Mazzotta, K. Dolag, S. Marri, Weighing simulated galaxy clusters using lensing and X-ray. *Astron. Astrophys.* **514**, 93 (2010b). doi:10.1051/0004-6361/200913222
- J. Miralda-Escude, A Test of the Collisional Dark Matter Hypothesis from Cluster Lensing. *ArXiv Astrophysics e-prints* (2000)
- J.J. Mohr, A.E. Evrard, D.G. Fabricant, M.J. Geller, Cosmological Constraints from Observed Cluster X-Ray Morphologies. *ApJ* **447**, 8 (1995). doi:10.1086/175852
- S.M. Molnar, I.-N. Chiu, K. Umetsu, P. Chen, N. Hearn, T. Broadhurst, G. Bryan, C. Shang, Testing Strict Hydrostatic Equilibrium in Simulated Clusters of Galaxies: Implications for A1689. **724**, 1–4 (2010). doi:10.1088/2041-8205/724/1/L1
- A. Morandi, S. Ettori, Entropy profiles in X-ray luminous galaxy clusters at z 0.1. **380**, 1521–1532 (2007). doi:10.1111/j.1365-2966.2007.12158.x
- A. Morandi, M. Limousin, Triaxiality, principal axis orientation and non-thermal pressure in Abell 383. **421**, 3147–3158 (2012). doi:10.1111/j.1365-2966.2012.20537.x
- A. Morandi, K. Pedersen, M. Limousin, Unveiling the Three-dimensional Structure of Galaxy Clusters: Resolving the Discrepancy Between X-ray and Lensing Masses. *Astrophys. J.* **713**, 491–502 (2010). doi:10.1088/0004-637X/713/1/491
- A. Morandi, K. Pedersen, M. Limousin, Reconstructing the Triaxiality of the Galaxy Cluster A1689: Solving the X-ray and Strong Lensing Mass Discrepancy. *Astrophys. J.* **729**, 37 (2011a). doi:10.1088/0004-637X/729/1/37
- A. Morandi, M. Limousin, J. Sayers, S.R. Golwala, N.G. Czakon, E. Pierpaoli, S. Ameglio, X-ray, lensing and Sunyaev Zel'dovich triaxial analysis of Abell 1835 out to R200. *ArXiv e-prints*(2011b)
- A. Morandi, M. Limousin, Y. Rephaeli, K. Umetsu, R. Barkana, T. Broadhurst, H. Dahle, Triaxiality and non-thermal gas pressure in Abell 1689. **416**, 2567–2573(2011b). doi:10.1111/j.1365-2966.2011.19175.x
- M.J. Mortonson, W. Hu, D. Huterer, Simultaneous falsification of Λ CDM and quintessence with massive, distant clusters. **83**(2), 023015 (2011). doi:10.1103/PhysRevD.83.023015
- J.C. Muñoz-Cuartas, A.V. Macciò, S. Gottlöber, A.A. Dutton, The redshift evolution of Λ cold dark matter halo parameters: concentration, spin and shape. **411**, 584–594 (2011). doi:10.1111/j.1365-2966.2010.17704.x
- A.F. Neto, L. Gao, P. Bett, S. Cole, J.F. Navarro, C.S. Frenk, S.D.M. White, V. Springel, A. Jenkins, The statistics of Λ CDM halo concentrations. **381**, 1450–1462 (2007). doi:10.1111/j.1365-2966.2007.12381.x
- A.B. Newman, T. Treu, R.S. Ellis, D.J. Sand, The Dark Matter Distribution in A383: Evidence for a Shallow Density Cusd Lensing, Stellar Kinematic, and X-ray Data. **728**, 39 (2011)

- A.B. Newman, T. Treu, R.S. Ellis, D.J. Sand, C. Nipoti, J. Richard, E. Jullo, The Density Profiles of Massive, Relaxed Galaxy Clusters: I. The Total Density Over 3 Decades in Radius. ArXiv e-prints(2012a)
- A.B. Newman, T. Treu, R.S. Ellis, D.J. Sand, The Density Profiles of Massive, Relaxed Galaxy Clusters: II. Separating Luminous and Dark Matter in Cluster Cores. ArXiv e-prints(2012b)
- P.D. Noerdlinger, The intrinsic flattening of galaxies. *ApJ* **234**, 802–809 (1979). doi:10.1086/157559
- M. Nord, K. Basu, F. Pacaud, P.A.R. Ade, A.N. Bender, B.A. Benson, F. Bertoldi, H.-M. Cho, G. Chon, J. Clarke, M. Dobbs, D. Ferrusca, N.W. Halverson, W.L. Holzzapfel, C. Horellou, D. Johansson, J. Kennedy, Z. Kermish, R. Kneissl, T. Lanting, A.T. Lee, M. Lueker, J. Mehl, K.M. Menten, T. Plagge, C.L. Reichardt, P.L. Richards, R. Schaaf, D. Schwan, H. Spieler, C. Tucker, A. Weiss, O. Zahn, Multi-frequency imaging of the galaxy cluster Abell 2163 using the Sunyaev-Zel'dovich effect. *Astron. Astrophys.* **506**, 623–636 (2009). doi:10.1051/0004-6361/200911746
- M. Oguri, R.D. Blandford, What is the largest Einstein radius in the universe? **392**, 930–944 (2009). doi:10.1111/j.1365-2966.2008.14154.x
- M. Oguri, M. Takada, K. Umetsu, T. Broadhurst, Can the Steep Mass Profile of A1689 Be Explained by a Triaxial Dark Halo? *Astrophys. J.* **632**, 841–846 (2005). doi:10.1086/452629
- M. Oguri, J.F. Hennawi, M.D. Gladders, H. Dahle, P. Natarajan, N. Dalal, B.P. Koester, K. Sharon, M. Bayliss, Subaru Weak Lensing Measurements of Four Strong Lensing Clusters: Are Lensing Clusters Overconcentrated? *Astrophys. J.* **699**, 1038–1052 (2009). doi:10.1088/0004-637X/699/2/1038
- M. Oguri, M. Takada, N. Okabe, G.P. Smith, Direct measurement of dark matter halo ellipticity from two-dimensional lensing shear maps of 25 massive clusters. **405**, 2215–2230 (2010). doi:10.1111/j.1365-2966.2010.16622.x
- M. Oguri, M.B. Bayliss, H. Dahle, K. Sharon, M.D. Gladders, P. Natarajan, J.F. Hennawi, B.P. Koester, Combined strong and weak lensing analysis of 28 clusters from the Sloan Giant Arcs Survey. **420**, 3213–3239 (2012). doi:10.1111/j.1365-2966.2011.20248.x
- N. Okabe, M. Takada, K. Umetsu, T. Futamase, G.P. Smith, LoCuSS: Subaru Weak Lensing Study of 30 Galaxy Clusters. **62**, 811 (2010)
- S.G. Patiri, A.J. Cuesta, F. Prada, J. Betancort-Rijo, A. Klypin, The Alignment of Dark Matter Halos with the Cosmic Web. **652**, 75–78 (2006). doi:10.1086/510330
- D.J. Paz, D.G. Lambas, N. Padilla, M. Merchán, Shapes of clusters and groups of galaxies: comparison of model predictions with observations. **366**, 1503–1510 (2006a). doi:10.1111/j.1365-2966.2005.09934.x
- D.J. Paz, D.G. Lambas, N. Padilla, M. Merchán, Shapes of clusters and groups of galaxies: comparison of model predictions with observations. *MNRAS* **366**, 1503–1510 (2006b). doi:10.1111/j.1365-2966.2005.09934.x
- E.-H. Peng, K. Andersson, M.W. Bautz, G.P. Garmire, Discrepant Mass Estimates in the Cluster of Galaxies Abell 1689. *Astrophys. J.* **701**, 1283–1299 (2009). doi:10.1088/0004-637X/701/2/1283
- A.H.G. Peter, M. Rocha, J.S. Bullock, M. Kaplinghat, Cosmological Simulations with Self-Interacting Dark Matter II: Halo Shapes vs. Observations. ArXiv e-prints (2012)
- R. Piffaretti, R. Valdarnini, Total mass biases in X-ray galaxy clusters. *Astron. Astrophys.* **491**, 71–87 (2008). doi:10.1051/0004-6361:200809739
- R. Piffaretti, P. Jetzer, S. Schindler, Aspherical galaxy clusters: Effects on cluster masses and g as mass fractions. *Astron. Astrophys.* **398**, 41–48 (2003). doi:10.1051/0004-6361:20021648
- M. Plionis, S. Basilakos, H.M. Tovmassian, The shape of poor groups of galaxies. *MNRAS* **352**, 1323–1328 (2004). doi:10.1111/j.1365-2966.2004.08023.x
- M. Postman, D. Coe, N. Benítez, L. Bradley, T. Broadhurst, M. Donahue, H. Ford, O. Graur, G. Graves, S. Jouvel, A. Koekemoer, D. Lemze, E. Medezinski, A. Molino, L. Moustakas, S. Ogaz, A. Riess, S. Rodney, P. Rosati, K. Umetsu, W. Zheng, A. Zitrin, M. Bartelmann, R. Bouwens, N. Czakon, S. Golwala, O. Host, L. Infante, S. Jha, Y. Jimenez-Teja, D. Kelson, O. Lahav, R. Lazkoz, D. Maoz, C. McCully, P. Melchior, M. Meneghetti, J. Merten, J. Moustakas, M. Nonino, B. Patel, E. Regös, J. Sayers, S. Seitz, A. Van der Wel, The Cluster Lensing and Supernova Survey with Hubble: An Overview. **199**, 25 (2012). doi:10.1088/0067-0049/199/2/25
- F. Prada, A.A. Klypin, A.J. Cuesta, J.E. Betancort-Rijo, J. Primack, Halo concentrations in

- the standard Λ cold dark matter cosmology. **423**, 3018–3030 (2012). doi:10.1111/j.1365-2966.2012.21007.x
- E. Puchwein, M. Bartelmann, Three-dimensional reconstruction of the intra-cluster medium. *Astron. Astrophys.* **455**, 791–801 (2006). doi:10.1051/0004-6361:20054717
- E. Rasia, S. Ettori, L. Moscardini, P. Mazzotta, S. Borgani, K. Dolag, G. Tormen, L.M. Cheng, A. Diaferio, Systematics in the X-ray cluster mass estimators. **369**, 2013–2024 (2006). doi:10.1111/j.1365-2966.2006.10466.x
- K. Reblinsky, Cluster deprojection combining multiple observable data sets. *Astron. Astrophys.* **364**, 377–390 (2000)
- M. Redlich, M. Bartelmann, J.-C. Waizmann, C. Fedeli, The strongest gravitational lenses: I. The statistical impact of cluster mergers. *ArXiv e-prints* (2012)
- S. Riemer-Sørensen, D. Paraficz, D.D.M. Ferreira, K. Pedersen, M. Limousin, H. Dahle, Resolving the Discrepancy Between Lensing and X-Ray Mass Estimates of the Complex Galaxy Cluster Abell 1689. *Astrophys. J.* **693**, 1570–1578 (2009). doi:10.1088/0004-637X/693/2/1570
- M. Rocha, A.H.G. Peter, J.S. Bullock, M. Kaplinghat, S. Garrison-Kimmel, J. Onorbe, L.A. Moustakas, Cosmological Simulations with Self-Interacting Dark Matter I: Constant Density Cores and Substructure. *ArXiv e-prints* (2012)
- G. Rossi, R.K. Sheth, G. Tormen, Modelling the shapes of the largest gravitationally bound objects. **416**, 248–261 (2011). doi:10.1111/j.1365-2966.2011.19028.x
- B.S. Ryden, The Intrinsic Shapes of Stellar Systems. *Astrophys. J.* **461**, 146 (1996). doi:10.1086/177043
- J. Samsing, A. Skielboe, S.H. Hansen, Measuring the Three-dimensional Shape of X-Ray Clusters. *Astrophys. J.* **748**, 21 (2012). doi:10.1088/0004-637X/748/1/21
- D.J. Sand, T. Treu, R.S. Ellis, The Dark Matter Density Profile of the Lensing Cluster MS 2137-23: A Test of the Cold Dark Matter Paradigm. **574**, 129–133 (2002). doi:10.1086/342530
- D.J. Sand, T. Treu, G.P. Smith, R.S. Ellis, The Dark Matter Distribution in the Central Regions of Galaxy Clusters: Implications for Cold Dark Matter. *Astrophys. J.* **604**, 88–107 (2004). doi:10.1086/382146
- D.J. Sand, T. Treu, R.S. Ellis, G.P. Smith, J.-P. Kneib, Separating Baryons and Dark Matter in Cluster Cores: A Full Two-dimensional Lensing and Dynamic Analysis of Abell 383 and MS 2137-23. *Astrophys. J.* **674**, 711–727 (2008). doi:10.1086/524652
- J. Sayers, S.R. Golwala, S. Ameglio, E. Pierpaoli, Cluster Morphologies and Model-independent Y_{SZ} Estimates from Bolocam Sunyaev-Zel’dovich Images. *Astrophys. J.* **728**, 39(2011a). doi:10.1088/0004-637X/728/1/39
- M. Sereno, On the deprojection of clusters of galaxies combining X-ray, Sunyaev-Zeldovich temperature decrement and gravitational lensing maps. **380**, 1207–1218 (2007). doi:10.1111/j.1365-2966.2007.12171.x
- M. Sereno, K. Umetsu, Weak- and strong-lensing analyses of the triaxial matter distribution of Abell 1689. **416**, 3187–3200 (2011). doi:10.1111/j.1365-2966.2011.19274.x
- M. Sereno, A. Zitrin, Triaxial strong-lensing analysis of the z 0.5 MACS clusters: the mass-concentration relation. **419**, 3280–3291 (2012). doi:10.1111/j.1365-2966.2011.19968.x
- M. Sereno, S. Ettori, A. Baldi, Shape and orientation of the gas distribution in A1689. **419**, 2646–2656 (2012). doi:10.1111/j.1365-2966.2011.19914.x
- M. Sereno, P. Jetzer, M. Lubini, On the overconcentration problem of strong lensing clusters. **403**, 2077–2087 (2010a). doi:10.1111/j.1365-2966.2010.16248.x
- M. Sereno, M. Lubini, P. Jetzer, A multiwavelength strong lensing analysis of baryons and dark matter in the dynamically active cluster AC 114. *Astron. Astrophys.* **518**, 55 (2010b). doi:10.1051/0004-6361/200913843
- M. Sereno, E. De Filippis, G. Longo, M.W. Bautz, Measuring the Three-dimensional Structure of Galaxy Clusters. II. Are Clusters of Galaxies Oblate or Prolate? *Astrophys. J.* **645**, 170–178 (2006). doi:10.1086/503198
- L.D. Shaw, J. Weller, J.P. Ostriker, P. Bode, Statistics of Physical Properties of Dark Matter Clusters. *Astrophys. J.* **646**, 815–833 (2006). doi:10.1086/505016
- L.D. Shaw, D. Nagai, S. Bhattacharya, E.T. Lau, Impact of Cluster Physics on the Sunyaev-Zel’dovich Power Spectrum. *Astrophys. J.* **725**, 1452–1465 (2010). doi:10.1088/0004-637X/725/2/1452
- J. Silk, S.D.M. White, The determination of Q_0 using X-ray and microwave observations of galaxy clusters. **226**, 103–106 (1978). doi:10.1086/182841

- A. Skielboe, R. Wojtak, K. Pedersen, E. Rozo, E.S. Rykoff, Spatial anisotropy of galaxy kinematics in SDSS galaxy clusters. ArXiv e-prints (2012)
- G.P. Smith, H. Ebeling, M. Limousin, J.-P. Kneib, A.M. Swinbank, C.-J. Ma, M. Jauzac, J. Richard, E. Jullo, D.J. Sand, A.C. Edge, I. Smail, Hubble Space Telescope Observations of a Spectacular New Strong-Lensing Galaxy Cluster: MACS J1149.5+2223 at $z = 0.544$. **707**, 163–168 (2009). doi:10.1088/0004-637X/707/2/L163
- G.P. Smith, H.G. Khosroshahi, A. Dariush, A.J.R. Sanderson, T.J. Ponman, J.P. Stott, C.P. Haines, E. Egami, D.P. Stark, LoCuSS: connecting the dominance and shape of brightest cluster galaxies with the assembly history of massive clusters. **409**, 169–183 (2010). doi:10.1111/j.1365-2966.2010.17311.x
- J. Sommer-Larsen, M. Limousin, Moderate steepening of galaxy cluster dark matter profiles by baryonic pinching. **408**, 1998–2007 (2010). doi:10.1111/j.1365-2966.2010.17260.x
- G. Soucail, B. Fort, Y. Mellier, J.P. Picat, A blue ring-like structure, in the center of the A 370 cluster of galaxies. *Astron. Astrophys.* **172**, 14–16 (1987)
- V. Springel, J. Wang, M. Vogelsberger, A. Ludlow, A. Jenkins, A. Helmi, J.F. Navarro, C.S. Frenk, S.D.M. White, The Aquarius Project: the subhaloes of galactic haloes. **391**, 1685–1711 (2008). doi:10.1111/j.1365-2966.2008.14066.x
- A.A. Stark, Triaxial Models of the Bulge of M31. *Astrophys. J.* **213**, 368–373 (1977). doi:10.1086/155164
- P. Thakur, D.K. Chakraborty, Correlated projected properties of some triaxial mass models: implications for their intrinsic shapes. *MNRAS* **328**, 330–338 (2001). doi:10.1046/j.1365-8711.2001.04794.x
- K. Umetsu, T. Broadhurst, Combining Lens Distortion and Depletion to Map the Mass Distribution of A1689. *Astrophys. J.* **684**, 177–203 (2008). doi:10.1086/589683
- K. Umetsu, M. Birkinshaw, G.-C. Liu, J.-H.P. Wu, E. Medezinski, T. Broadhurst, D. Lemze, A. Zitrin, P.T.P. Ho, C.-W.L. Huang, P.M. Koch, Y.-W. Liao, K.-Y. Lin, S.M. Molnar, H. Nishioka, F.-C. Wang, P. Altamirano, C.-H. Chang, S.-H. Chang, S.-W. Chang, M.-T. Chen, C.-C. Han, Y.-D. Huang, Y.-J. Hwang, H. Jiang, M. Kesteven, D.Y. Kubo, C.-T. Li, P. Martin-Cocher, P. Oshiro, P. Raffin, T. Wei, W. Wilson, Mass and Hot Baryons in Massive Galaxy Clusters from Subaru Weak-Lensing and AMiBA Sunyaev-Zel'Dovich Effect Observations. *Astrophys. J.* **694**, 1643–1663 (2009). doi:10.1088/0004-637X/694/2/1643
- K. Umetsu, T. Broadhurst, A. Zitrin, E. Medezinski, L.-Y. Hsu, Cluster Mass Profiles from a Bayesian Analysis of Weak-lensing Distortion and Magnification Measurements: Applications to Subaru Data. *Astrophys. J.* **729**, 127 (2011). doi:10.1088/0004-637X/729/2/127
- C.A. Vera-Ciro, L.V. Sales, A. Helmi, C.S. Frenk, J.F. Navarro, V. Springel, M. Vogelsberger, S.D.M. White, The shape of dark matter haloes in the Aquarius simulations: evolution and memory. **416**, 1377–1391 (2011). doi:10.1111/j.1365-2966.2011.19134.x
- A. Vikhlinin, A. Kravtsov, W. Forman, C. Jones, M. Markevitch, S.S. Murray, L. Van Speybroeck, Chandra Sample of Nearby Relaxed Galaxy Clusters: Mass, Gas Fraction, and Mass-Temperature Relation. *Astrophys. J.* **640**, 691–709 (2006a). doi:10.1086/500288
- A. Vikhlinin, A. Kravtsov, W. Forman, C. Jones, M. Markevitch, S.S. Murray, L. Van Speybroeck, Chandra Sample of Nearby Relaxed Galaxy Clusters: Mass, Gas Fraction, and Mass-Temperature Relation. *Astrophys. J.* **640**, 691–709 (2006b). doi:10.1086/500288
- J.-C. Waizmann, M. Redlich, M. Bartelmann, The strongest gravitational lenses: II. Is the large Einstein radius of MACS J0717.5+3745 in conflict with LCDM? ArXiv e-prints (2012)
- M.S. Warren, P.J. Quinn, J.K. Salmon, W.H. Zurek, Dark halos formed via dissipationless collapse. I - Shapes and alignment of angular momentum. *Astrophys. J.* **399**, 405–425 (1992). doi:10.1086/171937
- R.H. Wechsler, J.S. Bullock, J.R. Primack, A.V. Kravtsov, A. Dekel, Concentrations of Dark Halos from Their Assembly Histories. *Astrophys. J.* **568**, 52–70 (2002). doi:10.1086/338765
- J.S.B. Wyithe, E.L. Turner, D.N. Spergel, Gravitational Lens Statistics for Generalized NFW Profiles: Parameter Degeneracy and Implications for Self-Interacting Cold Dark Matter. *Astrophys. J.* **555**, 504–523 (2001). doi:10.1086/321437
- N. Yoshida, V. Springel, S.D.M. White, G. Tormen, Collisional Dark Matter and the Structure of Dark Halos. **535**, 103–106 (2000). doi:10.1086/312707
- K. Yoshikawa, Y. Suto, Reconstructing the Radial Profiles of Gas Density and Temperature in Clusters of Galaxies from High-Resolution X-Ray and Radio Observations. *Astrophys. J.* **513**, 549–554 (1999). doi:10.1086/306908
- Q. Yuan, T.-J. Zhang, B.-Q. Wang, Reconstruction of Gas Temperature and Density Profiles of the Galaxy Cluster RX J1347.5 1145. **8**, 671–676 (2008). doi:10.1088/1009-9271/8/6/05

-
- S. Zaroubi, G. Squires, Y. Hoffman, J. Silk, Deprojection of Rich Cluster Images. **500**, 87 (1998). doi:10.1086/311421
- S. Zaroubi, G. Squires, G. de Gasperis, A.E. Evrard, Y. Hoffman, J. Silk, Deprojection of Galaxy Cluster X-Ray, Sunyaev-Zeldovich Temperature Decrement, and Weak-Lensing Mass Maps. *Astrophys. J.* **561**, 600–620 (2001). doi:10.1086/323359
- Y.-Y. Zhang, N. Okabe, A. Finoguenov, G.P. Smith, R. Piffaretti, R. Valdarnini, A. Babul, A.E. Evrard, P. Mazzotta, A.J.R. Sanderson, D.P. Marrone, LoCuSS: A Comparison of Cluster Mass Measurements from XMM-Newton and Subaru: Testing Deviation from Hydrostatic Equilibrium and Non-thermal Pressure Support. *Astrophys. J.* **711**, 1033–1043 (2010). doi:10.1088/0004-637X/711/2/1033
- D.H. Zhao, Y.P. Jing, H.J. Mo, G. Börner, Mass and Redshift Dependence of Dark Halo Structure. **597**, 9–12 (2003). doi:10.1086/379734
- A. Zitrin, T. Broadhurst, Discovery of the Largest Known Lensed Images Formed by a Critically Convergent Lensing Cluster. **703**, 132–136 (2009). doi:10.1088/0004-637X/703/2/L132
- A. Zitrin, T. Broadhurst, Y. Rephaeli, S. Sadeh, The Largest Gravitational Lens: MACS J0717.5+3745 ($z = 0.546$). **707**, 102–106 (2009). doi:10.1088/0004-637X/707/1/L102
- A. Zitrin, T. Broadhurst, R. Barkana, Y. Rephaeli, N. Benítez, Strong-Lensing Analysis of a Complete Sample of 12 MACS Clusters at $z = 0.5$: Mass Models and Einstein Radii. ArXiv e-prints (2010)
- A. Zitrin, T. Broadhurst, M. Bartelmann, Y. Rephaeli, M. Oguri, N. Benítez, J. Hao, K. Umetsu, The universal Einstein radius distribution from 10 000 SDSS clusters. **423**, 2308–2324 (2012). doi:10.1111/j.1365-2966.2012.21041.x
- Lensing and x-ray mass estimates of clusters (simulations). *New Journal of Physics* **14**(5), 055018 (2012). doi:10.1088/1367-2630/14/5/055018